HHS Public Access

Author manuscript

Nat Microbiol. Author manuscript; available in PMC 2023 April 01.

Published in final edited form as:

Nat Microbiol. 2022 October ; 7(10): 1673–1685. doi:10.1038/s41564-022-01224-7.

Inflammation-associated nitrate facilitates ectopic colonization of oral bacterium *Veillonella parvula* in the intestine

Daniel F. Rojas-Tapias[#,1,2,6], **Eric M. Brown**[#,1,2], **Emily R. Temple**[1], **Michelle A. Onyekaba**[1], **Ahmed M. T. Mohamed**[1,2], **Kellyanne Duncan**[1,2], **Melanie Schirmer**[1,3], **Rebecca L. Walker**[1], **Toufic Mayassi**[1,2], **Kerry A. Pierce**[4], **Julián Ávila-Pacheco**[4], **Clary B. Clish**[4], **Hera Vlamakis**[1,5], **Ramnik J. Xavier**[1,2,5,*]

[1]Broad Institute of MIT and Harvard, Cambridge, MA, USA

[2]Center for Computational and Integrative Biology and Department of Molecular Biology, Massachusetts General Hospital, Boston, MA, USA

[3]Emmy Noether Group, ZIEL - Institute for Food and Health, Technical University of Munich, Freising, Bavaria, Germany

[4]Metabolomics Platform, Broad Institute of MIT and Harvard, Cambridge, MA, USA

[5]Center for Microbiome Informatics and Therapeutics, Massachusetts Institute of Technology, Cambridge, MA, US

[6]Current address: Department of Agricultural Microbiology, Colombian Corporation for Agricultural Research - Agrosavia, Bogotá, Colombia

Abstract

Colonization of the intestine by oral microbes has been linked to multiple diseases such as inflammatory bowel disease (IBD) and colon cancer, yet mechanisms allowing expansion in this niche remain largely unknown. *Veillonella parvula,* an asaccharolytic, anaerobic, oral microbe that derives energy from organic acids, increases in abundance in the intestine of patients with IBD. Here, we show that nitrate, a signature metabolite of inflammation, allows *V. parvula* to transition from fermentation to anaerobic respiration. Nitrate respiration, through the *narGHJI* operon, boosted *Veillonella* growth on organic acids and also modulated its metabolic repertoire, allowing it to use amino acids and peptides as carbon sources. This metabolic shift was accompanied by changes in carbon metabolism and ATP production pathways. Nitrate respiration was fundamental for ectopic colonization in a mouse model of colitis, as a *Veillonella narG* deletion mutant colonized significantly less than a wild-type strain during inflammation. These results suggest that *Veillonella* harnesses conditions present during inflammation to colonize in the intestine.

[*]Corresponding author: Ramnik J. Xavier, M.D., Ph.D. Massachusetts General Hospital, Richard B. Simches Research Center, 185 Cambridge Street, 7th floor, Boston, MA 02114, USA, xavier@molbio.mgh.harvard.edu.

[#]These authors contributed equally to this work

AUTHOR CONTRIBUTIONS

Conceptualization, D.F.R.-T., H.V., R.J.X.; Methodology, D.F.R.-T., E.M.B., E.R.T., K.A.P., J.A.-P.; Computational analyses, D.F.R.-T., M.S., R.L.W.; Investigation, D.F.R.-T., E.M.B., E.R.T., M.A.O., A.M.T.M., K.D., T.M., K.A.P.; Manuscript writing, D.F.R.-T., E.M.B., H.V., R.J.X.; Manuscript editing, all authors; Supervision, C.B.C., H.V., R.J.X.

COMPETING INTERESTS

The authors declare no competing interests.

INTRODUCTION

The oral cavity harbors the second largest and most diverse microbiota within the human body[1,2] and, along with the gut, forms the mouth-gut axis[3]. Interactions between microbes of these niches and the host are implicated in the pathogenesis of gastrointestinal diseases and chronic inflammation[3,4]. The presence of prototypical oral microbes, including *Veillonella* and *Fusobacterium,* in the intestinal mucosa is associated with multiple pathologies including IBD[5–8], colorectal cancer[9–11], and cystic fibrosis[12–14]. Ingestion of saliva is the main introduction of oral microbes into the gut environment, although oral microbes are usually poor gut colonizers and do not cause disease in healthy individuals[15]. *Klebsiella* species isolated from saliva of IBD patients, however, were identified as pathobionts whose ectopic intestinal colonization induces type 1 T helper (Th_1) cells[4].

Molecular mechanisms associated with shifts in oral and gut microbes during inflammation are poorly understood. Gut inflammation is accompanied by changes in a vast number of metabolites that can drive expansion or depletion of species[16–18]. For instance, inflammation elevates levels of reactive oxygen and nitrogen species (ROS and RNS) that kill select microbes, particularly strict anaerobes in close proximity to the epithelium. Inflammation therefore results in an altered gut milieu that could promote colonization by oral microbes.

Much of our understanding of molecular strategies adopted by microbes to invade the inflamed gut originates from model *Proteobacteria* species[19–22]. *Escherichia coli* gains a colonization advantage during inflammation through its ability to use formate as a carbon and energy source when coupled with oxygen respiration[20] and to use nitrate as a terminal electron acceptor[19]. *Salmonella enterica* serovar Typhimurium utilizes ethanolamine—unlike most gut microbes—and lactate as carbon sources when coupled with tetrathionate and oxygen respiration, respectively[22,23]. Under anaerobic conditions, *Salmonella* Typhi uses nitrate via a periplasmic nitrate reductase to grow in the intestinal lumen[24,25]. Less is known, however, about the physiology and ecology of strict anaerobes, owing to the lack of genetic tools to manipulate these organisms and the inherent complexity of the gut environment.

Veillonella are gram-negative, obligate anaerobes present in the human oral cavity that obtain energy by fermenting short-chain organic acids. They are normally found in biofilms and tend to co-aggregate with lactic acid bacteria[26–29] that produce lactate as a by-product, which serves as the main carbon and energy source for *Veillonella*[26,30,31]. In this study, we show that *Veillonella*, a prototypical member of the oral microbiome commonly enriched in the intestines of IBD patients[7,32], is capable of transitioning from fermentation to anaerobic respiration. We demonstrate that nitrate, a metabolite enriched during inflammation, is used by *Veillonella* strains as a terminal electron acceptor to expand their metabolic landscapes and boost growth. Using a reductionist approach, we elucidate the metabolic pathways that accompany this transition and enable *Veillonella* to colonize and persist in the inflamed gut. Our findings provide a framework to understand the increased abundance of *Veillonella* species in patients with IBD and other inflammatory conditions.

RESULTS

Gut inflammation is associated with *Veillonella* enrichment

Veillonella is implicated in the disease course of IBD patients[7,32]. To further illustrate *Veillonella* enrichment in the context of inflammation, we used longitudinal gut microbiome data from treatment-naive, pediatric ulcerative colitis (UC)[32] and Crohn's disease (CD)[33] studies. Abundances of *V. parvula and V. dispar* increased with increasing levels of fecal calprotectin, an inflammation marker, in UC patients (Fig. 1a). Comparing CD cases to non-IBD subjects revealed a similar increase with disease (Fig. 1b). We therefore hypothesized that gut injury and inflammation provides favorable conditions for expansion of *Veillonella* species.

Nitrate respiration expands *Veillonella*'s metabolic landscape

Veillonella is a member of the Fimicutes phylum that uses a fermentative metabolism to extract carbon and energy from only a few organic acids[34]. In certain strains, nitrate reductase activity was previously observed[35–38]. Given that nitrate is increased during inflammation and harnessed by some facultative anaerobic *Proteobacteria* in the gut[19,24], we hypothesized that inflammation-associated nitrate is used by *Veillonella* to expand in the inflamed gut. An unbiased search for the presence of genetic clusters involved in nitrate reduction within the membrane-bound respiratory (Nar), periplasmic dissimilatory (Nap), and cytoplasmic assimilatory (Nas) nitrate reductase families[39] confirmed the increased representation of these clusters in *Proteobacteria* compared to other gut microbes (Extended Data Fig. 1a). Moreover, homologs of these genes are uncommon in oral Firmicutes and Bacteroidetes as well as gut Firmicutes, Bacteroidetes, and Actinobacteria (Extended Data Fig. 1a–c). *Veillonella* species, however, contained a *nar* family nitrate reduction cluster (Fig. 1c; Extended Data Fig. 1c). As no other nitrate reductase homologs were detected in *Veillonella* genomes, this suggests that *Veillonella* can potentially perform anaerobic respiration using nitrate as the terminal electron acceptor.

The membrane-bound respiratory nitrate reductase cluster in *V. parvula* comprises two divergently-located operons that contain genes encoding a potential NarGHI quinol:nitrate oxidoreductase and NarK nitrate/nitrite transporter (*narRGHJI* and *narK* operons) (Fig. 1c). This cluster exhibits similar organization in most *Veillonella* species, suggesting a common origin and function (Fig. 1c). We used the genetically tractable *V. parvula* SKV38[40] as the wild-type (WT) strain to assess the role of nitrate on growth. While a complex medium (SK) alone was unable to support *V. parvula* growth, the addition of lactate or malate stimulated growth rates and final cell densities (Fig. 1d), as seen previously with pyruvate[36]. When the medium was supplemented with nitrate (SKN), we observed growth without any additional carbon source, suggesting that alternative carbon sources present in SK medium are used by *Veillonella* in the presence of nitrate (Fig. 1d). This phenotype was reproducible in other rich growth media (Extended Data Fig. 2a). Moreover, we observed higher cell densities and growth rates when nitrate was present with either lactate or malate as the carbon source (Fig. 1d). Nitrate utilization, therefore, enhances growth on organic acids and allows *Veillonella* to grow on non-canonical carbon sources.

To confirm the involvement of the *narGHJI* gene cluster in nitrate utilization, we generated a *narG::tet* deletion, which also likely inactivated *narHJI* genes. Genetic complementation with *narGHJI* genes was unsuccessful, but whole-genome sequencing analysis revealed no uncharacterized mutations in *narG::tet*. The *narG::tet* strain was unable to grow on SKN alone and boost growth with lactate and malate, demonstrating a defect in utilizing nitrate (Fig. 1d). To further test the role of NarGHI, we generated a *narI::chl* deletion lacking the γ-chain of the respiratory nitrate reductase. As expected, *narI::chl* fully phenocopied *narG::tet,* and its complementation with an ectopic copy of *narI* driven from the $P_{narRGHJI}$ promoter fully restored the WT phenotype (Extended Data Fig. 2b).

Transcription of the *narRGHJI* operon was also induced in response to nitrate (Fig. 1e). Notably, several clinical *Veillonella* isolates exhibited similar growth phenotypes in response to nitrate, suggesting similar metabolic strategies (Extended Data Fig. 2c). *V. parvula* reduced nitrate to nitrite, and at least one fraction of nitrite was further reduced to ammonia or incorporated into biomass (Extended Data Fig. 3a), consistent with the dual assimilatory and respiratory nature of nitrate reduction previously observed in *V. parvula*[36]. Growth was not enhanced when ammonium or nitrite was used instead of nitrate, irrespective of the carbon source (Extended Data Fig. 3b,c). Altogether, we conclude that *Veillonella* species containing this cluster are able to use nitrate for respiration in a NarGHI-dependent manner.

Nitrate respiration allows *Veillonella* growth on amino acids

Nitrate respiration allowed *V. parvula* to grow on SKN medium. Dissection of the carbon sources showed that yeast extract was essential for growth; however, when yeast extract was present, omitting casitone significantly reduced growth (Fig. 2a). We therefore hypothesized that *V. parvula* is capable of using amino acids and/or peptides as carbon sources.

To assess contributions of various carbon sources, we used the SK base (SKb) medium: 0.25% yeast extract plus SK salts. During nitrate respiration, a dose-dependent growth increase resulted from supplementation with various protein hydrolysates (Fig. 2b). Casamino acids, which contain primarily free amino acids, led to higher optical densities compared to more complex sources at most concentrations tested (Fig. 2b). Casamino acids and casitone also positively impacted growth of other *Veillonella* strains during nitrate respiration (Extended Data Fig. 4a). During fermentation (when nitrate was absent), *V. parvula* failed to grow in SKb supplemented with any of the protein hydrolysates (Fig. 2b), while addition of lactate or malate stimulated growth (Extended Data Fig. 4b).

We then analyzed the spent SK medium by LC-MS to investigate whether amino acids or peptides were depleted during growth, noting significant decreases in the amount of amino acids at different growth phases (Fig. 2c; Extended Data Fig. 5a,b; Supplemental Data File 1). Asp was consumed during the mid-exponential phase, while Glu, Gln and Asn were depleted during the late exponential phase only when lactate (a preferred carbon source) was absent. Solely Asp and Asn were capable of enhancing the biomass and growth rate of *V. parvula* during nitrate respiration, although some growth was also observed after a significant lag phase with Asp in the absence of nitrate (Fig. 2d). Asp also stimulated the growth of other *Veillonella* strains in the presence of nitrate (Extended Data Fig. 4a). Utilization of Glu and Gln, by contrast, likely requires other metabolic intermediates.

Many dipeptides were also consumed during the late exponential phase, mainly in the absence of lactate (Fig. 2e; Supplementary Data Files 1,2). Of the dipeptides we annotated and analyzed, those with long and charged amino acids such as Glu, Lys, or Arg at either terminus or the respective presence of Trp and Pro on the N- and C-terminus exhibited reduced consumption. When Ala-Ala, Gly-Asp, or Ala-Gln were tested as carbon sources in SKbN medium, growth increased with Gly-Asp (Fig. 2f). Deletion of proton-dependent Opt family peptide transporters (*optA::chl optB::tet* double mutant)[41] but not ATP-dependent Opp oligopeptide transporters[42] eliminated this effect (Fig. 2f at 10h), further implicating the use of dipeptides for growth during nitrate respiration. The *V. ratti* nitrate reductase cluster contains a putative peptidase-encoding gene (Fig. 1c), highlighting the connection between nitrate respiration and peptide consumption for growth.

Metabolic changes associated with nitrate respiration

To study metabolic strategies associated with fermentation and respiration as well as use of amino acids/peptides during nitrate respiration, we examined profiles of *Veillonella*'s major by-products: propionate and acetate[43]. Propionate is generated through decarboxylation of succinate, the by-product of fumarate reduction (Fig. 3a,b)[44]. Propionate concentrations were low during nitrate respiration regardless of the carbon source present (Fig. 3c,d), consistent with reduced succinate pathway activity previously observed in response to nitrate[45] and the reduced requirement of fumarate as the terminal electron acceptor. Lactate fermentation, however, resulted in elevated propionate levels (Fig. 3c,d).

Acetate is produced via oxidation and decarboxylation of pyruvate, which results in the formation of both ATP and presumably reducing power (Fig. 3a,b)[43,46–49]. During fermentation and nitrate respiration with lactate present, acetate concentration was elevated (Fig. 3c,d). In contrast, during nitrate respiration with amino acids/peptides (SKN), acetate concentration was dramatically decreased. Reduced acetate production during growth with amino acids/peptides compared to growth with lactate reflects not only a more gluconeogenic metabolism, but also a decrease in the generation of ATP via pyruvate (Fig. 3b). Diminished formation of by-products (propionate plus acetate) during respiratory growth with amino acids/peptides also implies that a comparatively larger fraction of carbon is likely available for biomass synthesis (Fig. 3e).

We next sought to understand which genes are differentially expressed in response to different growth conditions. First, we compared expression profiles of cells growing with lactate during fermentation (SKL) and nitrate respiration (SKLN), which represent likely environments encountered in the oral cavity and inflamed gut, respectively (Fig. 3f,g). Nitrate respiration resulted in upregulation of the nitrate reductase cluster, as well as pathways associated with synthesis of leucine, histidine, and heme; it also resulted in downregulation of fumarate hydratase and the methylmalonyl pathway (8-fold), which presumably led to decreased propionate formation from fumarate and succinate during anaerobic respiration. During nitrate respiration, *poxB*, which encodes a pyruvate:ubiquinone oxidoreductase that channels electrons to the respiratory chain, was upregulated 16-fold. Next, we compared the transcriptomes of nitrate-respiring cells growing with amino acids/peptides (SKN) or lactate (SKLN) to analyze responses to

distinct carbon sources during nitrate respiration (Fig. 3f,h). With amino acids/peptides, genes involved in utilization or transport of purines, amino acids, and peptides (*optB, opp1*) were upregulated, consistent with our previous observation that amino acids/peptides support *Veillonella* growth when nitrate is present (Fig. 2). Notably, the *atp* operon was also upregulated with amino acids/peptides, indicative of a more determinant role for oxidative phosphorylation (OP) in this condition.

Nitrate respiration affects ATP synthesis in *Veillonella*

To understand how nitrate respiration expands the metabolic repertoire of *V. parvula* and boosts its growth with preferred carbon sources, we assessed the roles of the proton motive force (PMF) and ATP synthesis pathways during various growth conditions. To study the PMF, we used the $DiOC_2$ dye that is transported into cells as a function of the electrochemical gradient, thus reflecting changes in membrane potential. Regardless of the carbon source, the presence of nitrate led to a marked increase in membrane potential in WT cells, which was dependent on a functional NarGHI complex (Fig. 4a). Treatment with the ionophore carbonyl cyanide m-chlorophenyl hydrazone (CCCP) dissipated the gradient (Extended Data Fig. 6a). The importance of the electrochemical gradient was further assessed using a second uncoupler of OP: 2,4-dinitrophenol (2,4-DNP; Fig. 4b). During lactate fermentation, 2,4-DNP treatment reduced biomass and growth rate, reflecting the necessity of an active PMF. In the presence of nitrate, addition of 2,4-DNP reduced biomass and growth rates with lactate and amino acids/peptides. The growth rate reduction was more dramatic during amino acid/peptide than lactate utilization, suggesting that growth at the expense of these carbon sources occurs under a more elevated membrane potential (Fig. 4b, left in Fig. 3b).

Dissipation of the proton gradient reduced growth in all conditions, implying that the PMF is critical for substrate transport via proton-dependent transporters or ATP synthesis via OP. To study the role of PMF, we first assessed lactate and Asp transport (Fig. 4c,d; Extended Data Fig. 6b,c). In resting cells without nitrate, both lactate and Asp were scarcely consumed; addition of nitrate, however, increased lactate but not Asp uptake (Extended Data Fig. 6b). Growing cells consumed lactate, which was further stimulated by nitrate (Fig. 4c). This enhancement was dependent on nitrate respiration, as the difference due to nitrate addition disappeared in *narG::tet* cells (Fig. 4d). It is, however, uncertain why *narG::tet* cells in the absence of nitrate consumed lactate more rapidly than WT cells. Asp was slightly consumed by growing cells, but nitrate addition had no effect (Fig. 4c). Using computational and functional analyses, we identified L-lactate permease (LldP), a homolog of the proton-dependent LldP in *E. coli,* as the lactate transporter in *Veillonella* (Extended Data Fig. 6d). Thus, nitrate respiration directly promotes *Veillonella* growth by facilitating the uptake of nutrients transported in a PMF-dependent manner.

We then assessed the importance of the PMF on ATP synthesis using a strain lacking ATP synthase (*atpBEFHAGDC::tet,* hereafter *atp::tet*), a multicomplex enzyme that couples ATP synthesis to proton transport into the cytoplasm (Fig. 5a). Cells lacking ATP synthase were unable to grow with lactate during fermentation, but grew nearly as well as WT during nitrate respiration (Fig. 5b). Nitrate allowed for *atp::tet* growth, yet no ATP could be

generated via OP, impling that with lactate, ATP is primarily produced via substrate-level phosphorylation (SLP). The PMF generated with nitrate, therefore, must be harnessed to facilitate substrate uptake. The *atp::tet* strain failed to grow under nitrate respiration with amino acids/peptides, reflecting a potential requirement for ATP synthase under these conditions (Fig. 5b). Deletion strains lacking the ε (*atpC::chl*) or β and ε (*atpDC::chl*) subunits of ATP synthase displayed similar phenotypes (Extended Data Fig. 7a).

To further understand the role of the PMF and the contributions of SLP and OP to ATP synthesis during fermentation and respiration, we measured ATP levels in WT and *atp::tet* cells. Cells were grown on SKLN medium to mid-exponential phase, then washed and resuspended in SK medium. ATP was measured before and after supplementation with lactate and/or nitrate. Lactate addition significantly increased ATP levels in WT but not *atp::tet* cells. Supplementation with lactate plus nitrate dramatically elevated ATP levels in both WT and *atp::tet* cells, further confirming that ATP is mostly produced via SLP when lactate is present (Fig. 5c). Supplementation with lactate plus nitrate produced only minor differences in ATP levels between the strains, demonstrating that the growth deficiency of *atp::tet* observed during lactate fermentation (Fig. 5b) was not related to its capacity to produce ATP but instead to limited lactate uptake (Extended Data Fig. 6c). This also suggests that during lactate fermentation, the reverse reaction of ATP synthase is likely required to generate the PMF and energize proton-dependent lactate uptake (Fig. 5a). With nitrate supplementation, *atp::tet* cells produced approximately half the ATP produced by WT cells (Fig. 5c at 20 and 40min). OP, therefore, is required for ATP synthesis when *Veillonella* utilizes amino acids/peptides for growth. This is consistent with greater induction of the *atp* operon when cells were grown with amino acids/peptides (Fig. 3f,g; Extended Data Fig. 7b).

Veillonella expansion during inflammation is nitrate-dependent

We next assessed the importance of this metabolic switch on the capability of *Veillonella* to colonize the inflamed intestine. First, we examined whether epithelial injury and colitis led to *V. parvula* expansion in a gnotobiotic mouse model. We treated mice pre-colonized with altered Schaedler flora (ASF) with either 3% dextran sulfate sodium (DSS) or control solution for 8 days and orally gavaged the mice with WT or *narG::tet* (2×10^9 colony-forming units, CFUs) on day four (Fig. 6a). Inflammation was evident in DSS-treated mice by inflammatory cytokine production, neutrophil expansion, and decreased body weight and colon length (Fig. 6b,c; Extended Data Fig. 8a–d). Inflammation also resulted in a dramatic increase in *Veillonella* abundance in stool, as determined by qPCR, while absolute 16S rRNA counts were unaffected (Fig. 6d, Extended Data Fig. 9a). Our previous *in vitro* experiments did not reveal any growth defects for *narG::tet* when nitrate was absent (Fig. 1b), allowing us to test the importance of nitrate respiration in *Veillonella* expansion during inflammation. The *narG::tet* strain also expanded during inflammation, but to a significantly lower abundance than WT (Fig. 6d). Similar results were obtained by counting CFUs in stool and colonic tissue from control- and DSS-treated mice (Extended Data Fig. 9b,c). *narG* was upregulated, providing further evidence for *in vivo* nitrate utilization (Fig. 6e). In mice colonized with WT *Veillonella,* DSS treatment resulted in a 2-fold increase in lactate concentration in colonic tissue (Extended Data Fig. 9d). However, we observed no upregulation of *Veillonella* genes associated with lactate metabolism or induced by lactate in

our RNA-sequencing data (*lldD, lldP, hisA, argB*) in DSS-treated mice (Extended Data Fig. 9e).

To further assess nitrate respiration *in vivo*, we performed a competition experiment in which ASF mice received a 1:1 ratio of WT(*chl*) and *narG::tet* strains at the same dose and time point as the single colonization experiment. WT(*chl*) is an otherwise identical WT strain except for a chloramphenicol resistance gene in the intergenic region of *narK* and *hemZ* to distinguish between the *Veillonella* strains. WT(*chl*) colonized to significantly higher levels than *narG::tet* in the inflamed gut, as assessed by qPCR (Fig. 6g). Reduced fitness of *narG::tet* during inflammation was further confirmed by assessing CFUs in stool and colonic tissue from control- and DSS-treated mice, where we observed a 10-fold difference in colonization between WT(*chl*) and *narG::tet* (Fig. 6h,i; Supplementary Fig. 1). WT *Veillonella* were at least 100-fold more abundant in DSS- than control-treated ASF mice (Fig. 6h,i), suggesting that inflammation facilitates engraftment or provides additional cues for expansion.

We then asked whether *Veillonella* was able to colonize mice with a more complex gut microbiome, reflecting the human gut that harbors other nitrate utilizers, and adapted our single colonization model to mice from a specific-pathogen-free (SPF) environment (Fig. 6a). Given higher colonization resistance in these mice, we orally gavaged them with WT or *narG::tet* three times (days 2, 4 and 6) before the experimental endpoint. DSS-treated mice again displayed decreased weight and colon length (Fig. 6j,k). The ability of WT *Veillonella* to expand in the intestine increased during inflammation and surpassed that of *narG::tet* (Fig. 6l). *Veillonella* colonization in the intestine of SPF mice was variable and required additional inoculations, reflecting increased resistance of a complex murine microbiome to a human-derived oral microbe.

To gain further insight into the role of inflammatory nitrate in *Veillonella* expansion, we compared *Veillonella* colonization in WT and inducible nitric oxide synthase (iNOS) knockout (KO) SPF mice. Previous studies indicated that free nitrate in the gut during inflammation is largely derived from iNOS activity in immune cells[50]. DSS treatment showed equal effects on the colon lengths of WT and iNOS KO mice (Extended Data Fig. 9f), but *Veillonella* abundance in the stool of iNOS-deficient mice was significantly reduced compared to WT mice (Fig. 6m), phenocopying colonization with *narG::tet* (Fig. 6d,l). Collectively, these results demonstrate that *Veillonella* utilizes inflammatory nitrate derived from iNOS activity in host cells to ectopically colonize the gut.

DISCUSSION

Inflammation is an overarching factor that determines the ability of extraintestinal microbes to colonize the gut. One transverse factor resulting in expansion of these microbes is emergence of new electron acceptors that enable anaerobic respiration. Yet, the molecular and physiological implications of these molecules in non-model microbes has been poorly explored. Our mechanistic study unveiled key strategies that *V. parvula,* and potentially other *Veillonella* species, use to exploit metabolic signatures of inflammation and ectopically colonize the intestine.

Ectopic colonization of *Veillonella* observed in IBD patients indicates that inflammation provides appropriate environmental signals for its enrichment. *Veillonella* is aerotolerant and thus well adapted to oxygenic regions of the inflamed gut and to the presence of ROS, potentially increasing its success in these conditions. Moreover, we found that, unlike other gut Firmicutes, *Veillonella* possesses a respiratory nitrate reductase that enables anaerobic respiration. Nitrate respiration not only boosted *Veillonella* growth on organic acids, but also allowed amino acids and peptides to be used as carbon and energy sources. A mouse model of colitis confirmed the importance of nitrate respiration for colonizing the inflamed gut, as inactivation of *V. parvula narG* or murine iNOS impaired colonization. Transition from the oral cavity to the inflamed gut, therefore, may be driven by this fermentation-to-respiration switch. A potential limitation of this observation is the abundance of other nitrate utilizers, such as *E. coli,* in the mouse may not be reflective of that in the human gut.

The switch to nitrate respiration augments the proton gradient, which enhances proton-dependent transport and increases ATP generation via OP. Additionally, it reduces use of fumarate and the succinate pathway[45]. Our findings support a model in which nitrate respiration allows *Veillonella* growth on amino acids and peptides via the generation of extra ATP through OP as well as through a reduction in carbon waste in the forms of acetate and propionate. Similarly, the increased electrochemical gradient likely energizes peptide and amino acid transport via proton-coupled transporters, such as OptB[41]. Increased formation of ATP via ATP synthase using the energy of the PMF compensates for reduced energy formation via both SLP and the Na^+-driven gradient.

During inflammatory conditions *in vivo*, nitrate respiration increases *Veillonella* growth and hence its ability to compete and establish in the gut environment. Expansion of *Veillonella's* metabolic repertoire enables utilization of more diverse carbon sources, conferring an extra ability to colonize alternative niches. Small molecules (>3kDa) released from the death of gut epithelial cells were shown to promote growth of multiple intestinal Enterobacteriaceae[51]. In other oral microbes, such as *P. gingivalis*, the use of amino acids and peptides represents a virulence factor that allows colonization of inflamed tissue[52]. *Veillonella* might also potentially consume lactate that accumulates in tissues during inflammation[53] and is consistently observed to be enriched in IBD patients[17]. Although OP was less important in the presence of lactate, we hypothesize that it is also harnessed for ATP synthesis in settings where lactate is abundant. Additionally, increased PMF during nitrate respiration can be used to enhance the uptake efficiency of molecules mobilized via proton-dependent transporters, therefore facilitating growth in the gut environment. Discerning the relevant carbon sources *in vivo* and their implications for colonization remain to be explored.

V. parvula and other oral microbes are linked with multiple inflammatory diseases[32]. Our approach not only allowed us to confirm the positive correlation between inflammation and *Veillonella* abundance observed in IBD patients, but also to unravel the mechanistic strategies that underlie the transition from fermentation to nitrate respiration and allow for successful colonization of the inflamed gut. The capacity of *Veillonella* to alternate between different metabolic pathways highlights the versatility of the bacterial world, and additional microbes enriched during inflammatory conditions likely use parallel strategies. The fact

that *Veillonella*, as well as some Proteobacteria, use inflammatory nitrate to boost growth implies that reducing inflammation or the abundance of these microbes may interrupt the positive feedback between inflammation and dysbiosis.

MATERIALS AND METHODS

Analysis of human gut microbiome samples

The PROTECT cohort generated gut microbial profiles from pediatric UC patients[32]. We extracted the abundances of all operational taxonomic units (OTUs) assigned to *Veillonella* species from the published OTU abundance profiles (*V. dispar* OTU 342427, *V. parvula* OTU 518743, *V. parvula* OTU 3889756). Fecal calprotectin (FC) values were binned into low (<100 mcg/g), increased (100–200), high (200–3,000), and very high (>3,000). A two-sided Wilcoxon test was applied to compare the abundance of *V. parvula* and *V. dispar* across the 4 bins. Only samples where the respective OTU was present were included: *V. dispar* OTU 342427 was present in 1,006 samples, *V. parvula* OTU 518743 in 874 samples, and *V. parvula* OTU 3889756 in 487 samples.

The RISK study profiled pediatric CD patients[33]. We extracted the abundances of all *Veillonella* OTUs at species level from the published abundance profiles (*V. parvula* OTU 1755, *V. dispar* OTU 39) and compared their abundance in CD patients to non-IBD controls using a two-sided Wilcoxon test. Only samples where the respective OTU was present were included: *V. parvula* OTU 1755 was present in 529 samples, *V. dispar* OTU 39 in 846 samples.

Strains and culture media

Veillonella parvula SKV38 was used as the wild-type strain for our experiments. We also used *V.parvula* DSM2008, *V. dispar* LD205, *V. atypica* RJX1392, *V. atypica* RJX1514, and *V. ratti* 84 (Supplementary Table 1). Cells were grown routinely in SK agar (composition in g/L: yeast extract 10, casitone 10, Na_2HPO_4 0.4, NaCl 2.0) supplemented or not with DL-lactate (25 mM) and/or potassium nitrate (20 mM) unless otherwise indicated. The media with both lactate and nitrate added we called SKLN. Cells were incubated for 24 h under anaerobic conditions at 37°C. The growth of SKV38 was also assessed in GIFU anaerobic medium (HiMedia, Cat# M1801), Difco™ Reinforced Clostridium medium (BD Cat# 218081), DifcoTM Columbia broth (BD, Cat# 294420), MRS broth (Sigma, Cat# 69966), and BHI medium (HiMedia Cat# M210). Antibiotics were added to the medium when appropriate: 5 μg ml^{-1} tetracycline, 5 μg ml^{-1} chloramphenicol, 20 μg ml^{-1} erythromycin for *V. parvula*, and 100 μg ml^{-1} ampicillin and 100 μg ml^{-1} spectinomycin for *E. coli*. X-Gal (5-bromo-4-chloro-3-indolyl-β-D-galactopyranoside) was dissolved in DMSO (40 mg/ml), and added to plates for white/blue selection at a final concentration of 0.1 mg/ml.

Molecular biology techniques

The assembly of DNA fragments was routinely performed using Golden Gate cloning. For this, we used the plasmid pDRT004, which was constructed in this study, and allowed the modular assembly of DNA fragments. This plasmid contained BsaI and BbsI restriction

sites, respectively, surrounding a *lacZ* gene for blue/white selection and the ampicillin resistance gene. For gene knockout, two fragments of DNA flanking the gene of interest were amplified by PCR (~0.5 – 1.0 kb), and assembled with an antibiotic resistance gene (*tet*, *ery*, or *chl*) in pDRT004. The *tet* resistance gene was obtained from the pBSLJ1 plasmid, whereas the *chl* and *ery* genes under control of the *gyrA* promoter were synthesized as DNA fragments (IDT Technologies) (Supplementary Table 2) and cloned into pDRT004 as pDRT004 + *narG*(*chl*) and pDRT004 + *narG*(*ery*) for routine amplification of the resistance genes using primers DR096 and DR097. A typical 20 µl Golden Gate assembly reaction contained 2 µl of T4 DNA ligase buffer, 100 ng of pDRT004, equimolar amounts of the resistance gene (i.e. erythromycin, chloramphenicol or tetracycline whose transcription is driven from the P_{gyrA} promoter) and the two homology regions, 1.5 µl of BsaI HFv2 (NEB), 0.5 µl of T4 DNA ligase (NEB), and ultrapure water up to 20 µl. The reaction was incubated at 37°C for 1 h, and 60°C for 5 min. The Golden Gate reaction was then transformed into NEB Turbo competent *E. coli*, and the white colonies were selected for further experiments. For transformation of *V. parvula* SKV38, the assembled DNA fragments encompassing the homology regions and the resistance gene were amplified by PCR, and the PCR products were used for transformation. Mutations were verified by PCR and Sanger sequencing. Multiple clones were selected to assess phenotypes. In all cases, the DNA fragments were amplified using the Phusion™ high-fidelity DNA polymerase (Thermo F530S). All primers were purchased from Genewiz (USA), and the sequences are provided in Supplementary Table 3.

Veillonella parvula natural transformation

For genetic manipulation of *V. parvula*, we used natural transformation in SKL medium. Briefly, cells were grown overnight on SKLN medium agar plates, and cells from multiple colonies were resuspended to an OD_{600} ~ 0.400 in SK medium. A volume of 45 µl of the bacterial suspension was combined with 250–500 ng of DNA in a final volume of 50 µl. The DNA for this reaction was obtained by PCR amplification of the assembled vectors, as described above. Three 15 µl drops were then placed on SKL solid medium (previously autoclaved and poured under aerobic conditions) and incubated for 24 h at 37 °C under anaerobic conditions. Next day, one drop was resuspended in 50 µl of SK medium and plated on SKLN medium supplemented with the appropriate antibiotics (i.e. tetracycline 5 µg ml^{-1}, chloramphenicol 5 µg ml^{-1}, erythromycin 20 µg ml^{-1}). Colonies were visible after 24–48 h of incubation. Colonies were restreaked on SKLN medium containing antibiotics, and the mutations were verified by PCR and sequencing. DL-lactate (25 mM), nitrate (20 mM), and/or antibiotics were added after autoclaving. Plates were air dried for 48 h at 37 °C under aerobic conditions. For double or triple deletion mutants, the same protocol described above was used, but a deletion strain was used as the recipient strain for transformation. The antibiotic resistance profile, PCR, and sequencing were carried out to verify the genotypes.

Growth experiments

To study the impact of organic acids, amino acids, dipeptides, and peptones on growth of SKV38, we used the SK base broth (composition in g/L: yeast extract 2.5 (Sigma), Na_2HPO_4 0.4 (Sigma), NaCl 2.0 (Sigma)). KNO_3 (40 mM) (Sigma) was included or not as required. The composition of this medium was chosen as it permits the growth of *V. parvula*

up to OD_{600}~0.2, but further growth can be achieved by supplementation with other carbon sources. For the experiments, cells were grown overnight in SK with 40 mM nitrate. The next day, cells were washed twice in SK salts (composition in g/L: Na_2HPO_4 0.4, NaCl 2.0), and resuspended in the same buffer. The optical density of the suspension was measured, and the cultures inoculated at an initial OD_{600} of 0.025. Growth was monitored for 24 h by following OD_{600} in a BioTek Synergy H1. Sodium nitrite (Sigma), ammonium chloride (Sigma) were also used. The following carbon sources were used over the course of the experiment: L-lactate (Sigma), L-(−)-malic acid disodium salt (Sigma), sodium succinate (Sigma), sodium fumarate (Sigma), sodium pyruvate (Sigma). For assessment of the carbon sources in the other *Veillonella* strains, the SK base medium was modified as follows (in g/L): yeast extract 5.0, Na_2HPO_4 0.4, NaCl 2.0.

Maximum-specific growth rate (μ_{max}) values were determined from absorbance growth curves using the Exponential model (Eq. 1)[54], where ABS_t is absorbance at time t, k is a constant, μABS is the μ_{max} determined from absorbance measurements using the Exponential model (h^{-1}), and t is time (h). Absorbance values were taken during exponential growth.

$$Ln(ABS_t) = k \quad \mu ABS \cdot \quad t \qquad \text{(Eq. 1)}$$

Evaluation of growth with amino acids and complex peptides

To determine the capability of SKV38 to grow on amino acids, we used the SK base medium. The following amino acids were studied final concentration of 50 mM from stocks of 200 mM at pH ~ 7.0: L-aspartic acid (Sigma), L-glutamic acid potassium salt (Sigma), L-asparagine (Sigma), L-glutamine (Sigma). Casaminoacids (0.5%) (Calbiochem), Bacto™-Casitone (0.5%) (BD), tryptone (Sigma), Bacto™ peptone (BD), and yeast extract (Sigma) were also included for comparison. For this experiment, cells were grown on SK medium supplemented with 20 mM KNO_3. The next day, cells were collected by centrifugation at 10,000 × g, washed twice with 1X SK buffer, and resuspended in 1X SK buffer; OD_{600} was recorded and adjusted to 0.025. The experiment was monitored by spectrophotometry over a period of 24 h.

Gene expression analysis: RT-qPCR

Cells (1.5 ml) were harvested at the specific time points, centrifuged at 15,000 × g for 2 min under anaerobic conditions, the supernatant discarded, and finally the pellet resuspended in 0.6 ml of Trizol (Zymo). The suspensions were stored at −80 °C for further analysis. The cellular suspension was next combined with 1 g of zirconium beads and placed on a Tissue Lyser for cell disruption. RNA was then harvested using the Direct-zol RNA kit (Zymo) with in-column DNase treatment following manufacturer's instructions. RNA was eluted in 50 μl of ultrapure water. Synthesis of cDNA was performed using the iScript™ cDNA synthesis kit (Bio-Rad) following the instructions of the manufacturer. qPCR was performed using the iTaq Universal SYBR Green Supermix (Bio-Rad). Primers were designed using Primer3 v. 0.4.0 (https://primer3.ut.ee) and listed in Supplementary Table 4. The gene *gyrA* was used as reference.

Phylogenetic analyses of nitrate reductase genes

To test for detection of nitrate reductase genes in the human microbiome, we searched for species containing the gene in the assembled gene catalog from Pasoli et al (2019)[55], which consists of 9,428 metagenomes from different body sites, ages, countries, and lifestyles. The *E. coli narG* and *napA*, and *Klebsiella oxytoca nasA* amino acid sequences were queried against the gene catalog using USEARCH v8.1 "search_global" command[56]. Genes with at least 45% amino acid similarity and that originated from either stool or oral cavity samples were used for downstream analysis. To place the genomes containing a nitrate reductase gene on a phylogenetic tree, we used PhyloPhlAn v3.0.51 with default settings including all genomes containing at least one of the nitrate reductase genes[57].

Generation and analysis of RNA-sequencing data

Illumina cDNA libraries were generated using a modified version of the RNAtag-seq protocol[58]. Briefly, 500–1000 ng of total RNA was fragmented, depleted of genomic DNA, dephosphorylated, and ligated to DNA adapters carrying 5'-AN8–3' barcodes of known sequence with a 5' phosphate and a 3' blocking group. Barcoded RNAs were pooled and depleted of rRNA using the RiboZero rRNA depletion kit (Illumina). Pools of barcoded RNAs were converted to Illumina cDNA libraries in 2 main steps: (1) reverse transcription of the RNA using a primer designed to the constant region of the barcoded adaptor with addition of an adapter to the 3' end of the cDNA by template switching using SMARTScribe (Takara Bio)[59]; and (2) PCR amplification using primers whose 5' ends target the constant regions of the 3' or 5' adaptors and whose 3' ends contain the full Illumina P5 or P7 sequences. cDNA libraries were sequenced on the Illumina NovaSeq 6000 platform to generate paired end reads and collected using NovaSeq Control Software 1.6.

Sequencing reads from each sample in a pool were demultiplexed based on their associated barcode sequence using custom scripts. Up to 1 mismatch in the barcode was allowed provided it did not make assignment of the read to a different barcode possible. Barcode sequences were removed from the first read as were terminal Gs from the second read that may have been added by SMARTScribe during template switching. Reads were aligned to NZ_LR778174.1 using the Burrows-Wheeler Alignment tool (BWA) version 0.7.15-r1142-dirty[60] and read counts were assigned to genes and other genomic features using custom scripts. Differential expression analysis was conducted with edgeR v3.15[61]. Visualization of raw sequencing data and coverage plots in the context of genome sequences and gene annotations was conducted using GenomeView v2600[62].

Metabolite analysis

WT cells were grown until mid- and late exponential phase in SK medium supplemented or not with lactate and/or nitrate until they reached an OD_{600} ~0.3–0.4. A volume of 1.5 ml of the culture was then collected, centrifuged at 15,000 × g for 3 min, and 1.0 ml of the supernatant collected. This volume was then diluted 10 times and filter-sterilized for further analysis. For determination of organic acids, amino acids, and dipeptides, we used two liquid chromatography tandem mass spectrometry (LC-MS) methods designed to measure polar metabolites[63]. Briefly, amino acids and dipeptides were estimated using hydrophilic interaction liquid chromatography (HILIC) and an LC-MS system comprised of a Shimadzu

Nexera X2 U-HPLC (Shimadzu Corp., Marlborough, MA) coupled to a Q Exactive mass spectrometer (Thermo Fisher Scientific, Waltham, MA). Metabolites were extracted from media samples (10 μL) using 90 μL of acetonitrile/methanol/formic acid (74.9:24.9:0.2 v/v/v) containing stable isotope-labeled internal standards (valine-d8, Sigma-Aldrich, St. Louis, MO; phenylalanine-d8, Cambridge Isotope Laboratories, Andover, MA). The samples were centrifuged (9,000 × g, 4°C, 10 min), and the supernatants were injected directly onto a 150 × 2 mm, 3 μm Atlantis HILIC column (Waters, Milford, MA). MS analyses were carried out using electrospray ionization in the positive ion mode using full scan analysis over 70–800 m/z at 70,000 resolution. For the measurement of propionate HILIC and MS in negative ionization mode were conducted using an Shimadzu Nexera X2 U-HPLC (Shimadzu Corp., Marlborough, MA) coupled to a Q Exactive Plus mass spectrometer (Thermo Fisher Scientific, Waltham, MA). Metabolites were extracted from media (30 μL) using 120 μL of 80% methanol containing inosine-^{15}N4, thymine-d4 and glycocholate-d4 internal standards (Cambridge Isotope Laboratories, Andover, MA). The samples were centrifuged (10 min, 9,000 × g, 4°C), and the supernatants were injected directly onto a 150 × 2.0 mm Luna NH2 column (Phenomenex, Torrance, CA). MS analyses were carried out using electrospray ionization in the negative ion mode using full scan analysis over m/z 70–750 at 70,000 resolution and 3 Hz data acquisition rate. Additional MS settings were: ion spray voltage, −3.0 kV; capillary temperature, 350°C; probe heater temperature, 325 °C; sheath gas, 55; auxiliary gas, 10; and S-lens RF level 50. Compound identification was carried out by matching the retention time and m/z of feature in the data with an in-house collection of authentic standards including a library of 336 dipeptides (Anaspec AS-65126–336, Fremont, CA). Absolute quantitation of propionate was conducted using calibration curves spiked into media with stable isotope-labeled ^{13}C propionate (Cambridge Isotope Labs CLM-771 and CLM-627, Tewksbury, MA). Acetate (Sigma, MAK086), aspartate (Sigma, MAK095), glutamate (Sigma, MAK004), and nitrate / nitrite (Sigma, 482655) were determined using enzymatic assays, following the procedure recommended by the manufacturer. Raw data were processed using TraceFinder version 5.0 (Thermo Fisher Scientific, Waltham, MA) and Progenesis QI version 1.0 (Nonlinear Dynamics, Newcastle upon Tyne, UK). Extracted ion chromatograms for peaks of interest were generated and inspected using Thermo Scientific Xcalibur v. 4.3.

Measurement of the proton motive force

The membrane potential was assessed using the BacLight™ Bacterial Membrane Potential Kit (Invitrogen). Briefly, WT cells were grown on SK + 50 mM DL-lactate + 40 mM KNO_3 or SK + 50 mM L-malate + 40 mM KNO_3 broth until they reached mid-exponential phase (OD ~ 0.3–0.4). Next, cells were washed twice in SK medium, and resuspended at the same optical density in 1) SK + 50 mM DL-lactate, 2) SK + 50 mM DL-lactate + 40 mM nitrate, 3) SK + 50 mM L-malate, 4) SK + 50 mM L-malate + 40 mM nitrate, 5) SK, and 6) SK + 40 mM nitrate. After 45 min of incubation, cells were collected, diluted in 1 ml of filtered PBS (1/50 dilution), and treated or not with 10 μl of CCCP. Next, 10 μl of the $DiOC_2$ dye were added, the reaction incubated for 30 min, and fluorescence measured by flow cytometry.

2,4 – DNP experiments

Cells were grown overnight in SK medium supplemented with 20 mM nitrate and 25 mM lactate. The next day, the culture was centrifuged at 10,000 × g and rinsed twice with SK medium. Growth curves were then initiated in the presence of different concentrations of 2,4-dinitrophenol (2,4-DNP). The stock of 2,4-DNP was prepared at 100 mM in DMSO.

Lactate and aspartate consumption in growing and resting cells

The dynamics of sodium L-lactate (Sigma) and L-Asp (Sigma) consumption in growing and resting cells were studied in SKV38 WT cells. For this, cells were grown overnight on SK medium supplemented with 25 mM DL-lactate and 20 mM KNO_3. The next day, a new culture was started in SK + 50 mM DL-lactate + 40 mM KNO_3 medium, inoculated with 1/40 of the ON culture, and incubated for ~3–4 h until cells reached an OD_{600} = 0.3–0.4 under anaerobic conditions. Cells were collected by centrifugation at 10,000 × g, washed twice with phosphate-buffered saline (PBS), and resuspended in RC buffer (0.1 M potassium phosphate buffer pH 6.5, 20 mM $MgSO_4$, 20 mM beta-mercaptoethanol) for resting cells[64] or SK medium for growing cells. Absorbance was measured and adjusted to a final OD_{600} = 2.0 in a volume of 500 µl. After 40 min of incubation to deplete the pool of ATP, L-lactate, L-aspartate, and/or nitrate were added to the reaction. Samples of 20 µl were taken at specific time points, diluted with 480 µl of MiliQ water, centrifuged at 15,000 × g for 3 min, and the supernatant used for analytical determinations. Lactate was determined using the Lactate Determination Kit (Sigma, Cat# MAK064), and aspartate was determined using the Aspartate Determination Kit (Sigma, Cat# MAK095) following the instructions of the manufacturer.

ATP measurements

To measure ATP levels, cells were grown up to the mid-exponential phase, washed twice, and resuspended in the SK medium at an OD_{600} = 0.300. Cells were incubated for 40 min at 37°C to deplete intracellular ATP, and then lactate and/or nitrate added at the defined concentrations. ATP and optical density (600 nm) were simultaneously monitored after −10, 0, 20, 40, and 60 min. For this, 250 µl samples were combined with 100 µl ice-cold 3 M perchloric acid and incubated on ice for 2 h. Sterile medium was used as a control. Then, the pH was neutralized by the addition of 100 µl of 3 M KOH and 120 µl of 1.0 M Tes-NaOH buffer pH 7.0. The reaction was mixed by vortexing and centrifuged at 15,000 × g at 4 °C for 3 min. A volume of 400 µl of the supernatants were collected and kept at −20 °C for ATP determination. ATP determination was performed using the ATP Determination Kit (Invitrogen, Cat #A22066) based on the luciferase assay and following the manufacturer's recommendations. Luminescence was measured after 3 min of incubation. The concentration of ATP in the cells was determined by using a calibration curve with increasing concentrations of ATP.

Mouse experiments

All mouse experiments were performed according to protocols approved by the Institutional Animal Care and Use Committees (IACUC) of the Broad Institute and complied with all relevant ethical regulations. Mice were fed an autoclavable diet *ad libitum* (Lab Diet,; cat#

0001326) and housed with a 12-hour light/dark cycle at an ambient temperature between 18–24°C and 30–70% relative humidity. Mice were randomized into experimental groups; the number of mice utilized in each experiment is indicated in the figure legends.

Gnotobiotic mice colonized with altered Schaedler flora (ASF) used in experiments were C57BL/6N females or males aged 6–10 weeks and maintained in the germ-free facility at the Broad Institute. These mice were maintained with ASF for several generations. ASF mice in the DSS groups were given 3% dextran sulfate sodium salt (Mr approx. 40,000 kDa) in drinking water. After 4 days of DSS treatment, mice were orally gavaged with 100 μL of *Veillonella* culture at 2×10^{10} CFU/mL and continued DSS treatment for an additional 4 days post-gavage. DSS was removed and replaced with water for one day before sacrifice. For the specific-pathogen-free (SPF) model, we utilized male C57BL/6J mice from the Jackson Laboratories aged 8–10 weeks. We used both the WT strain (strain # 000664) and a strain deficient in iNOS activity (strain #002609; B6.129P2-*Nos2*^{tm1Lau}/J). SPF mice were gavaged with *Veillonella* as above iteratively on days 2, 4 and 6. SPF mice were given DSS as above for 7 days; DSS was removed and replaced with water for two days before sacrifice. Mice not receiving DSS treatment were gavaged with the appropriate *V. parvula* SKV38 WT or *narG::tet* strain at the same time and the same amount as DSS-treated mice. *Veillonella* cultures were prepared by setting up fresh cultures without antibiotics that were grown until OD_{600} reached 0.4–0.5 (~4 hours). Cells were washed in PBS and concentrated three times in an anaerobic chamber and finally diluted to reach $OD_{600} = 10$, which is equivalent to 2×10^{10} CFU/mL in both WT and *narG::tet* strains.

Lactate quantification in mouse tissue

Lactate quantification in mouse tissues was performed using a colorimetric assay kit (abcam Cat# ab65331), as per the manufacturer's instructions. For this, 10–20 mg of colonic tissue were homogenized in 1 ml of PBS, and 50 μl collected for lactate determination. Lactate values were normalized per mg of mouse tissue.

Lymphocyte isolation and flow cytometry

Epithelial cells were first stripped via mechanical disruption in RPMI (Gibco) containing 2 mM EDTA (Corning) and 1% fetal bovine serum (Gibco) for 45 min. Lamina propria lymphocytes were then obtained via subsequent mechanical disruption of remaining tissue in RPMI (Gibco) containing 0.5 mg/mL Collagenase VIII (Sigma) and 20% fetal bovine serum (Gibco) for 1 hr. The following conjugated antibodies were used to identify cellular markers: CD45 BUV805 (30-F11) (Bd Biosciences), Ly6G BV605 (1A8) (Biolegend), and Ly6C efluor450 (HK1.4) (Thermo-Fischer). All antibodies were used at a 1/400 dilution. Cells were analyzed on a Cytek Aurora cytometer (Cytek Biosciences). FlowJo 10.8.0. was used for analysis.

Cytokine assays

For *ex vivo* quantification of cytokine secretion, mesenteric lymph node cells were isolated in complete tissue culture media (RPMI, 10% FBS, 1% glutamine and 1% of 1:1 penicillin/streptomycin) and cultured in 96-well plates at 100,000 cells per well in 200 uL for 18 hours at 37°C, 5% carbon dioxide. The resulting supernatants were used to

determine the amount of each cytokine using murine-specific cytokine bead array kit for mouse inflammatory cytokines (Biolegend), relative to a standard curve, according to the manufacturer's recommendations.

Quantification of viable bacteria

Stool and colonic tissue collected from ASF mice colonized with *Veillonella* were weighed and homogenized in a buffer of 0.05% cysteine in PBS. Homogenates were serially diluted from 10^{-3} to 10^{-8} in sterile, deep-well 96-well plates. To assess colonization of *Veillonella*, resulting dilutions were plated on SKLN media with 5 μg/mL chloramphenicol for the WT strain and 10 μg/mL tetracycline for the *narG::tet* strain. Plates were incubated at 37°C under anaerobic conditions for 2 days. Colonies were counted and sent for 16S rRNA sequencing to confirm *Veillonella* was counted for each mouse. Colonies were considered below the limit of detection (nd) if no countable colonies were present at the 10^{-3} dilution factor.

Veillonella colonization assessment by qPCR

Stool from ASF and SPF mice colonized with *Veillonella* were collected and frozen immediately on dry ice. DNA was extracted using the PowerFecal Pro DNA extraction kit (Qiagen) following the manufacturer's instructions. All extracted DNA was normalized to the same concentration between different samples and experimental conditions before being used. The assessment of *Veillonella* abundance was performed using the iTaq Universal SYBR Green Supermix (Bio-Rad) and primers listed in Supplementary Table 4. The 16S rRNA gene was used as a reference gene for abundance. PCR was performed on an Applied Biosystems 7500 machine; cycles consisted of 95 °C for 15 min and 40 cycles of 95 °C for 15 s and 60 °C for 1 min. Relative expression compared to 16S rRNA was calculated using the $\Delta\Delta C(t)$ method. In the competition experiment, relative expression was calculated by directly comparing Ct values of the *chl* and *tet* genes in the WT(*chl*) and *narG::tet* strains, respectively.

Statistical analysis

For each experiment, cell sampling and the number of independent replicates are indicated in figure legends, along with the corresponding statistical test used. Power analysis was not formally conducted, however sample sizes were chosen based on previous experience and published literature. Parametric distributions of the data were tested and statistical tests used appropriately depending on the presence of a normal distribution. Data were analyzed with either a Student's *t*-test to compare two conditions with normal distributions, or a Mann-Whitney *U*-test for two conditions without normal distributions. For assessing statistical significance among three or more groups, a one-way ANOVA and Tukey's honestly significant difference (HSD) test or Dunnett's test was utilized as indicated. The *n* number reported in each figure legend refers to biological replicates. Data collection and analysis were not blinded due to the nature of the experimental designs in this study, but unbiased quantifications were applied to obtain the results. No data points were excluded from the analysis. Statistical analysis was performed with assistance from R versions 3.5 and 4.1 or GraphPad Prism version 9.0. Statistical significance is given as P values in the figures, where NS (not significant) indicates $P \geq 0.05$. Results are expressed as the mean value with standard error of the mean (SEM), unless otherwise indicated

Extended Data

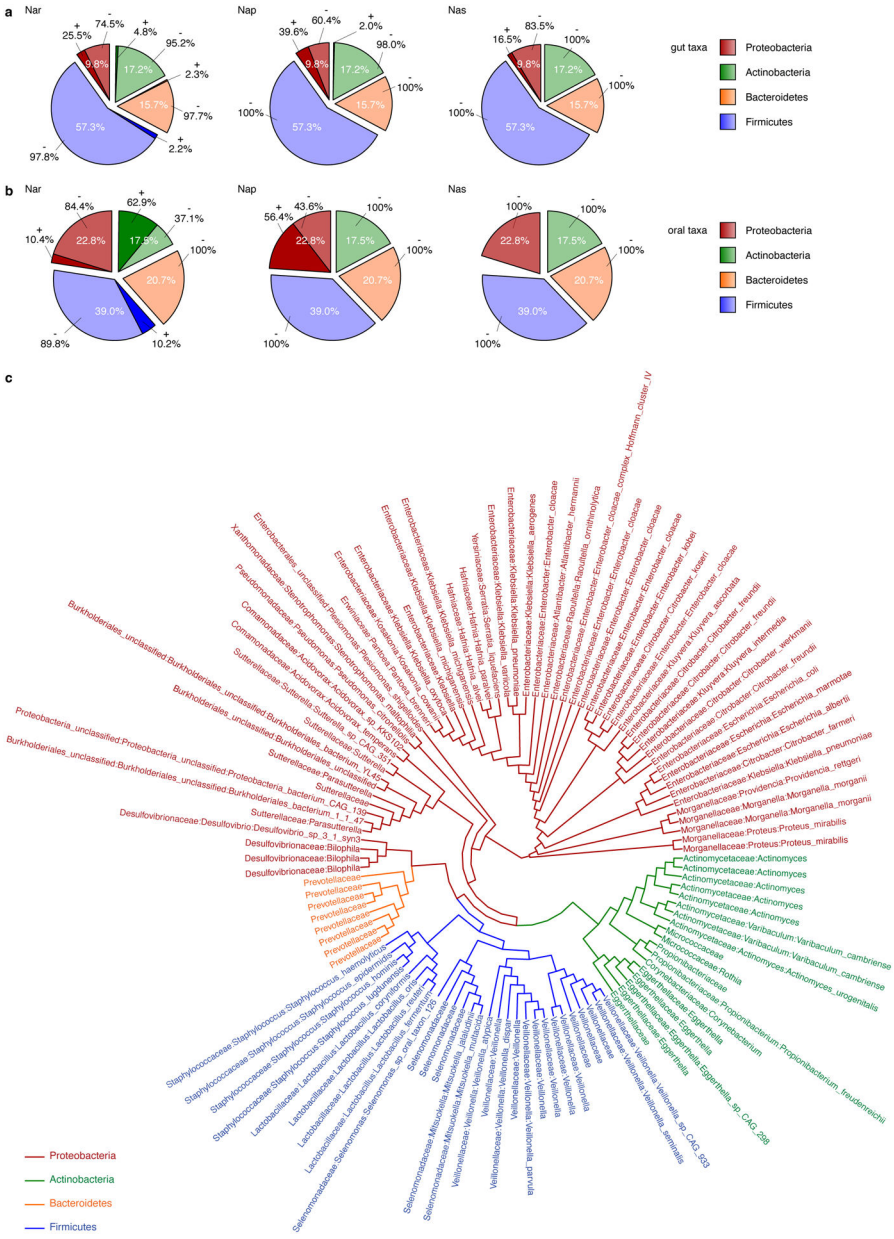

Extended Data Figure 1. Phylogenetic analysis of nitrate reductases.

Analysis of the Nar, Nap, and Nas nitrate reductase families in human **a)** gut and **b)** oral microbes, using the NarG and NapA protein sequences of *E. coli*, and NasA of *K. pneumoniae* as templates. The sequences were searched in the assembled gene catalog from Pasolli *et al.* (2019)[55]. **c)** Phylogenetic tree of NarG in gut microbes reveals that *Veillonella* is one of the few genera within the Firmicutes with a putative nitrate reductase. Genes with at least 45% amino acid similarity were used for analysis.

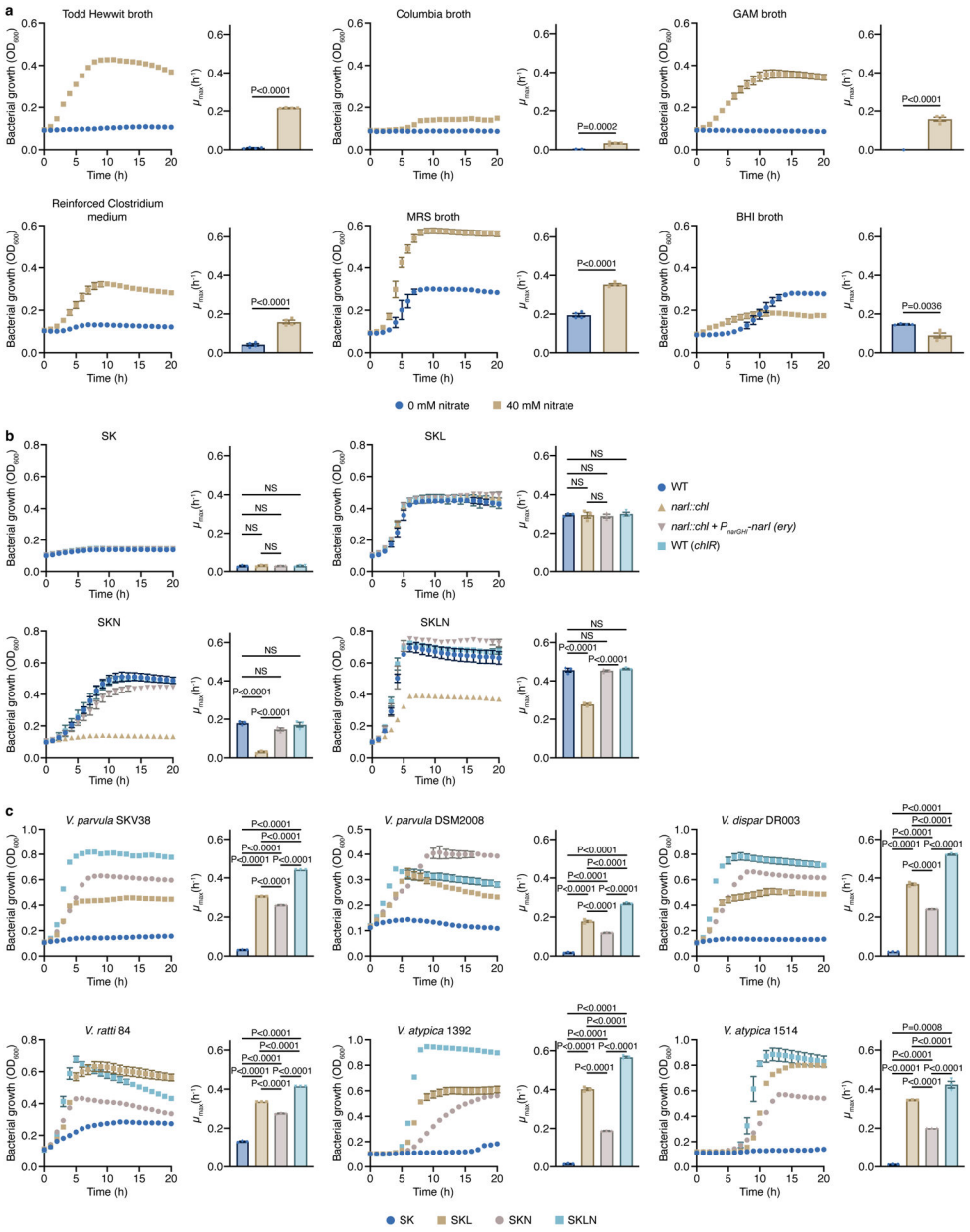

Extended Data Figure 2. Nitrate-stimulated growth of various *Veillonella* strains, and *narI::chl* complementation experiments.

a) The growth of *V. parvula* SKV38 was assessed in different complex media supplemented or not with 40 mM nitrate (n=4 biological replicates). **b)** Growth curves of WT and *narI::chl* strains in SK, SKL, SKN, and SKLN media. Cells lacking the NarI protein are unable to grow in SKN, and nitrate does not stimulate its growth when lactate is present (n=3 biological replicates). **c)** The growth of various *Veillonella* strains was assessed in SK, SKL, SKN, and SKLN media (n=3 biological replicates). Growth rates (μ_{max}) were calculated for each growth curve. Data (**a-c**) represent mean ± SEM, analyzed by one-way ANOVA and Tukey's HSD test. NS, not significant.

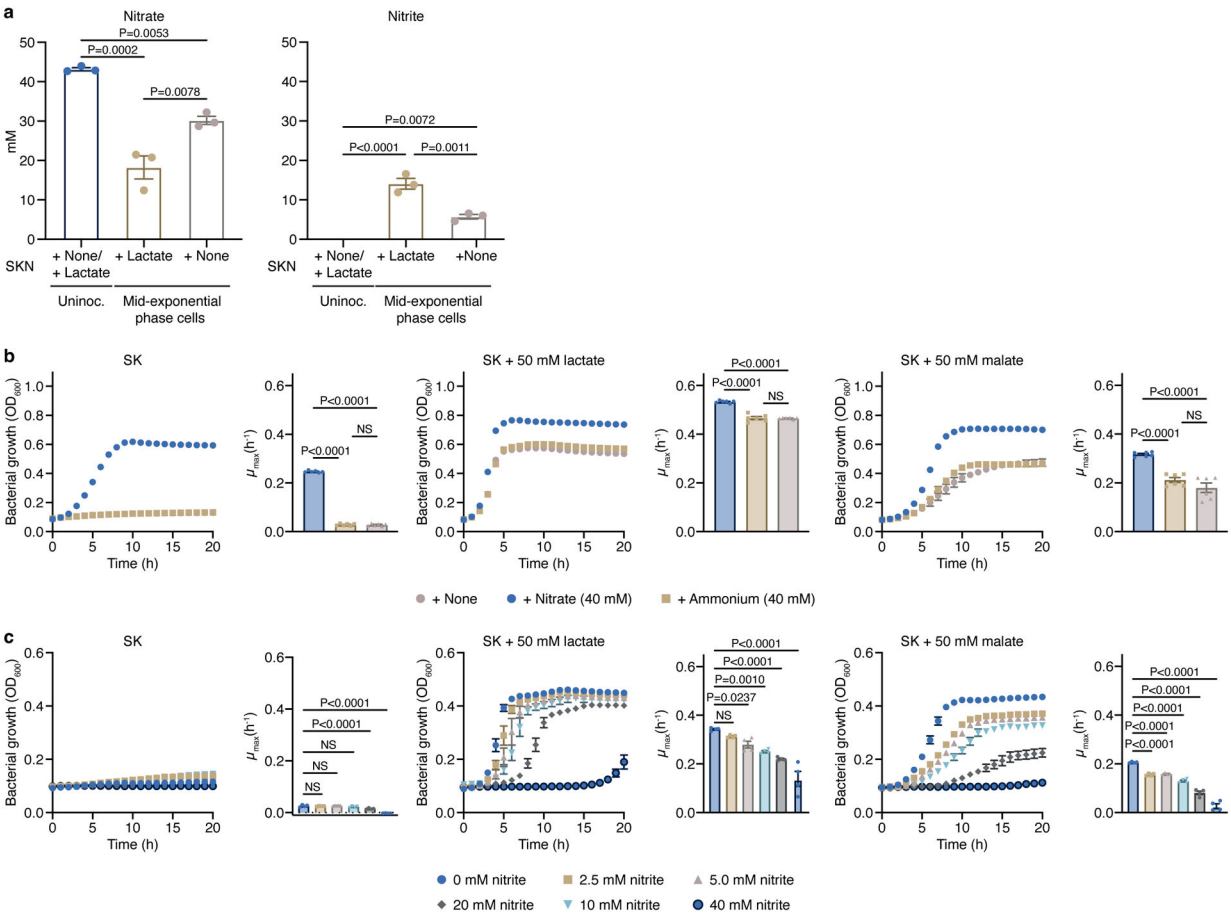

Extended Data Figure 3. Nitrate metabolism in *Veillonella*.

a) Levels of nitrate and nitrite were measured at the mid-exponential phase in cells growing on SKN medium supplemented or not with lactate as the carbon source (n=3 biological replicates). The measured concentrations of nitrate and nitrite in the uninoculated SK medium were 43.161 ± 0.410 mM and <0.050 mM, respectively (n=3 biological replicates). **b)** Ammonium (n=6 biological replicates) or **c)** nitrite (n=4 biological replicates) were used to determine if the positive effect of nitrate on growth of *V. parvula* was due to nitrate being used as a source of nitrogen or an electron acceptor, respectively. Growth rates (μ_{max}) were calculated for each growth curve. Data represent mean ± SEM, analyzed by one-way ANOVA and Tukey's HSD test (**a,b**) or Dunnett's test (**c**). NS, not significant.

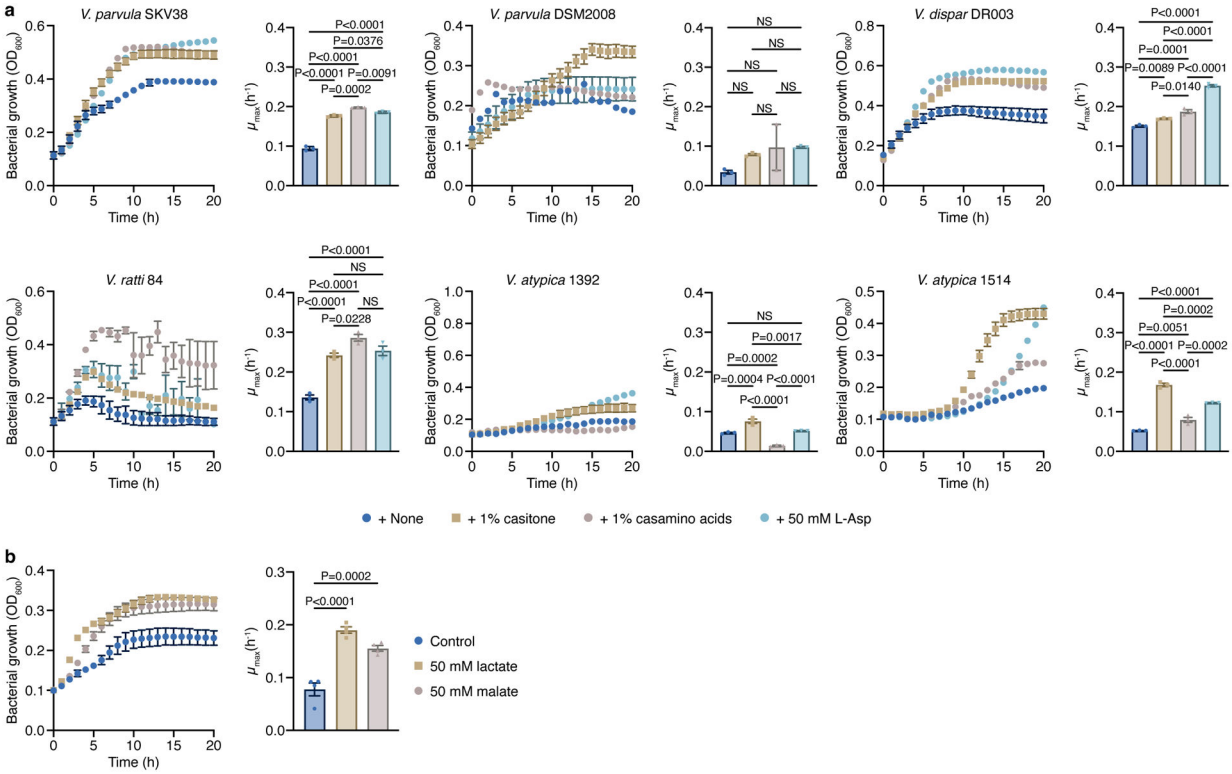

Extended Data Figure 4. Amino acids and peptides stimulate the growth of different *Veillonella* strains.

a) The growth of various *Veillonella* strains was studied in SKbN with 0.5% yeast extract, and with and without 1% casitone, 1% casamino acids, or 50 mM L-aspartic acid (n=3 biological replicates). **b)** The addition of lactate or malate stimulates growth of *V. parvula* in SKb medium (n=4 biological replicates). Growth rates (μ_{max}) were calculated for each growth curve. Data represent mean ± SEM, analyzed by one-way ANOVA and Tukey's HSD test (**a**) or Dunnett's test (**b**). NS, not significant.

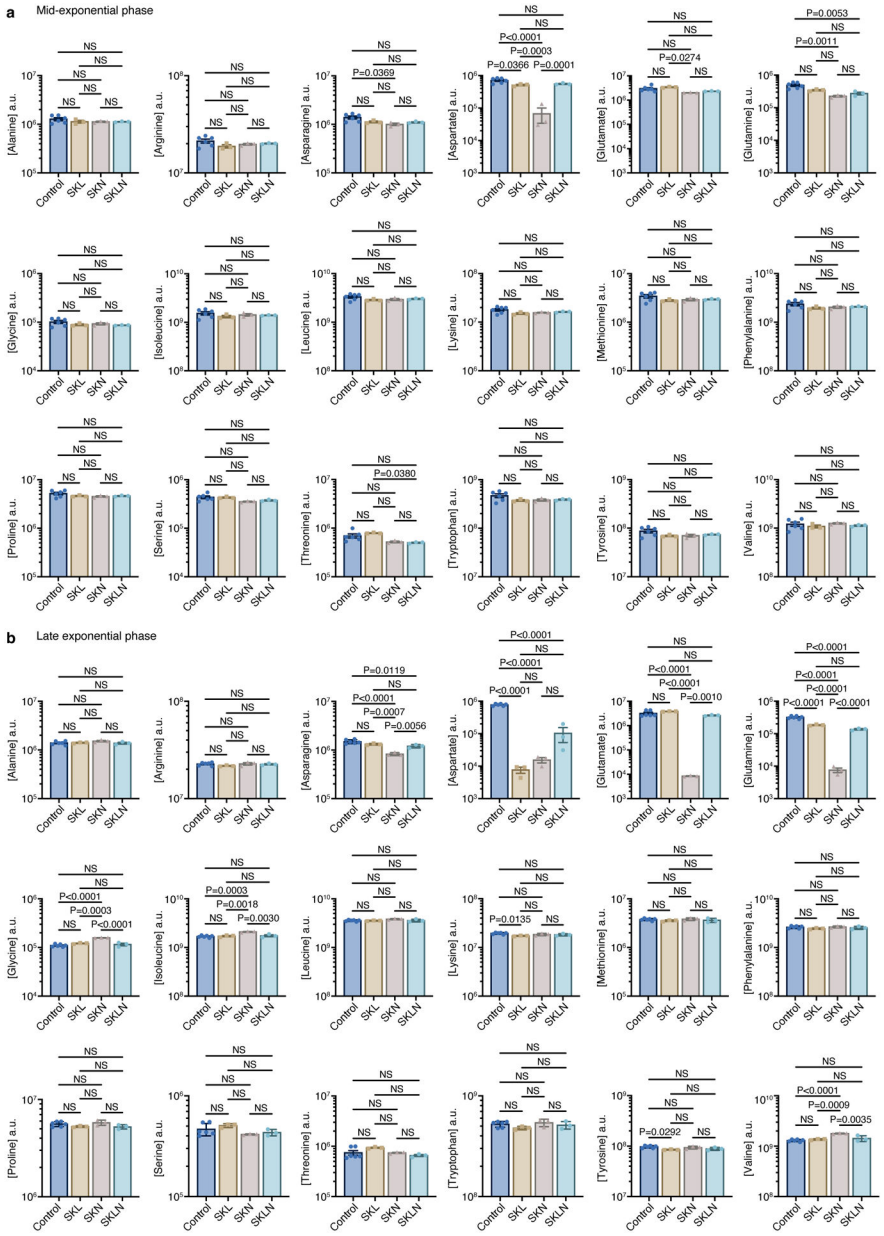

Extended Data Figure 5. LC-MS analysis of amino acids in unspent and spent media.

LC-MS analysis of the unspent (n=6 biological replicates) and spent SKL, SKN, and SKLN media (n=3 biological replicates) was used to study amino acid consumption. Supernatants were collected at the **a)** mid-exponential and **b)** late exponential phases. Data represent mean ± SEM, analyzed by one-way ANOVA and Tukey's HSD test. NS, not significant.

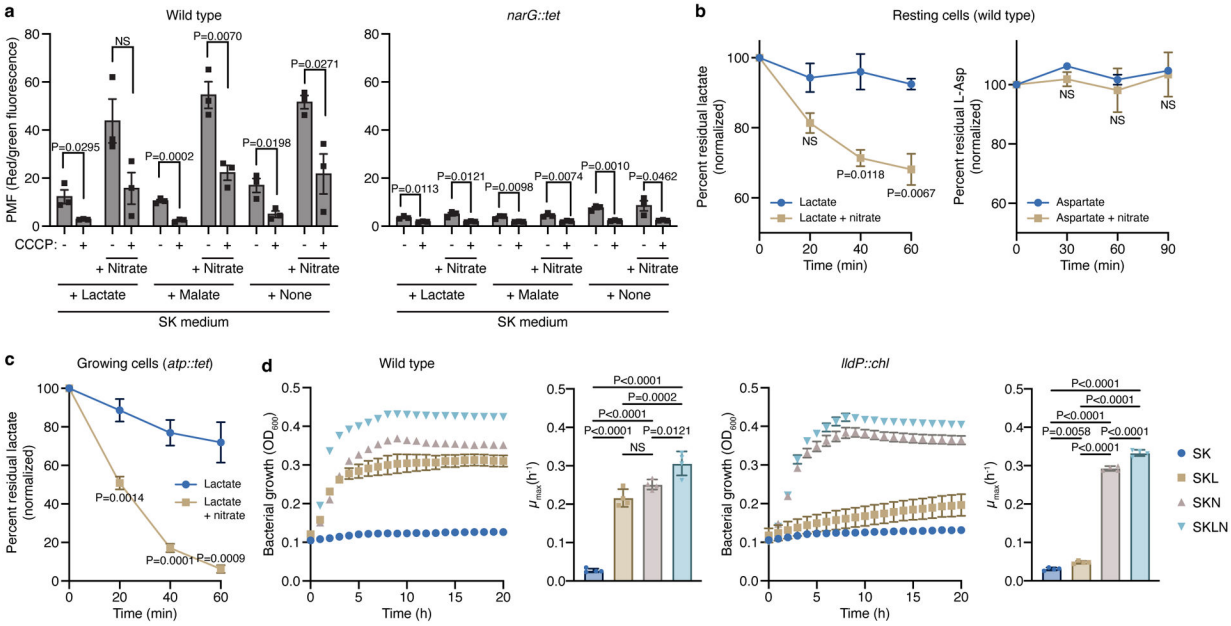

Extended Data Figure 6. Role of the PMF in the production of ATP and transport, and phenotype of the L-lactate permease (*lldP::chl*) mutant.

a) Measurement of the proton motive force (PMF) in WT and *narG::tet* cells growing on SK with and without lactate or malate, and with or without CCCP. The PMF was measured before and 40 min after addition of 40 mM nitrate. CCCP was added to confirm that the observed changes were associated with the proton gradient (n=3 biological replicates). **b)** Lactate (n=3 biological replicates) and aspartate (n=2 biological replicates) consumption were measured in resting WT cells resuspended in resting cell (RC) buffer with or without nitrate. **c)** Lactate consumption (n=4 biological replicates) was measured in growing *atp::tet* cells with or without nitrate. Both metabolites were measured in the supernatant using colorimetric techniques. **d)** Growth experiments with WT *Veillonella* and a strain lacking LldP *(lldP::chl)* in SK, SKL, SKN, and SKLN media (n=4 biological replicates). Cells lacking the LldP transporter are nearly unable to grow with lactate as the carbon source. Growth rates (μ_{max}) were calculated for each growth curve. Data (**a-d**) represent mean ± SEM, analyzed by two-sided *t*-test (**a, b**, and **c**), or one-way ANOVA and Tukey's HSD test (growth rates in **d**). NS, not significant.

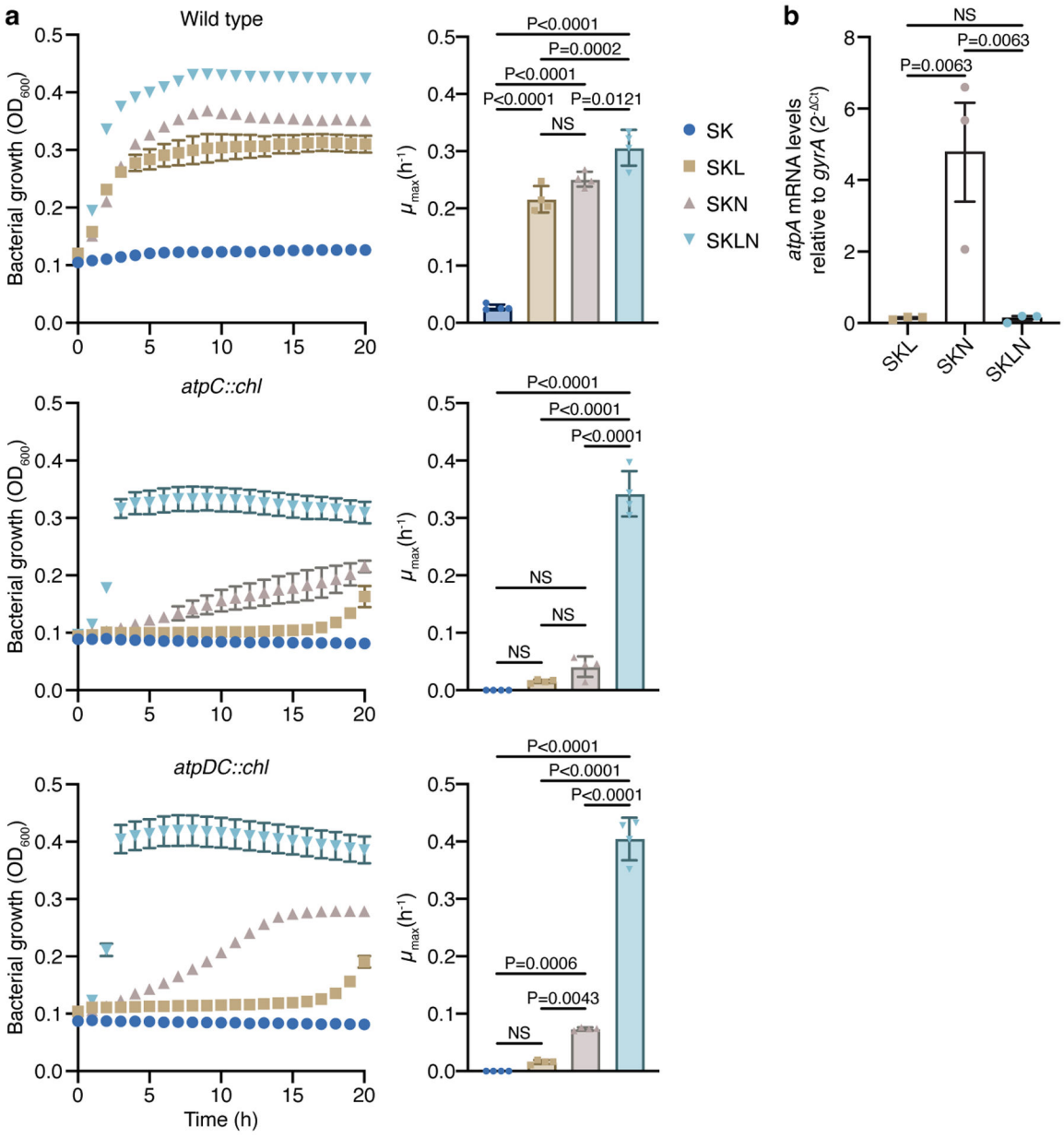

Extended Data Figure 7. Phenotype of cells lacking components of the ATP synthase, and expression analysis of the *atp* operon.

a) Growth experiments with WT *Veillonella* and the AtpC *(atpC::chl)* and AtpD-AtpC (*atpDC::chl*) deletion strains in SK, SKL, SKN, and SKLN media (n=4 biological replicates). These deletion strains exhibited a phenotype similar to the one seen in the *atp::tet* strain. Growth rates (μ_{max}) were calculated for each growth curve. **b)** Transcriptional analysis of the *atpA* gene in cells growing in SKL, SKN, and SKLN media (n=3 biological replicates). Data represent mean ± SEM, analyzed by one-way ANOVA and Tukey's HSD test. NS, not significant.

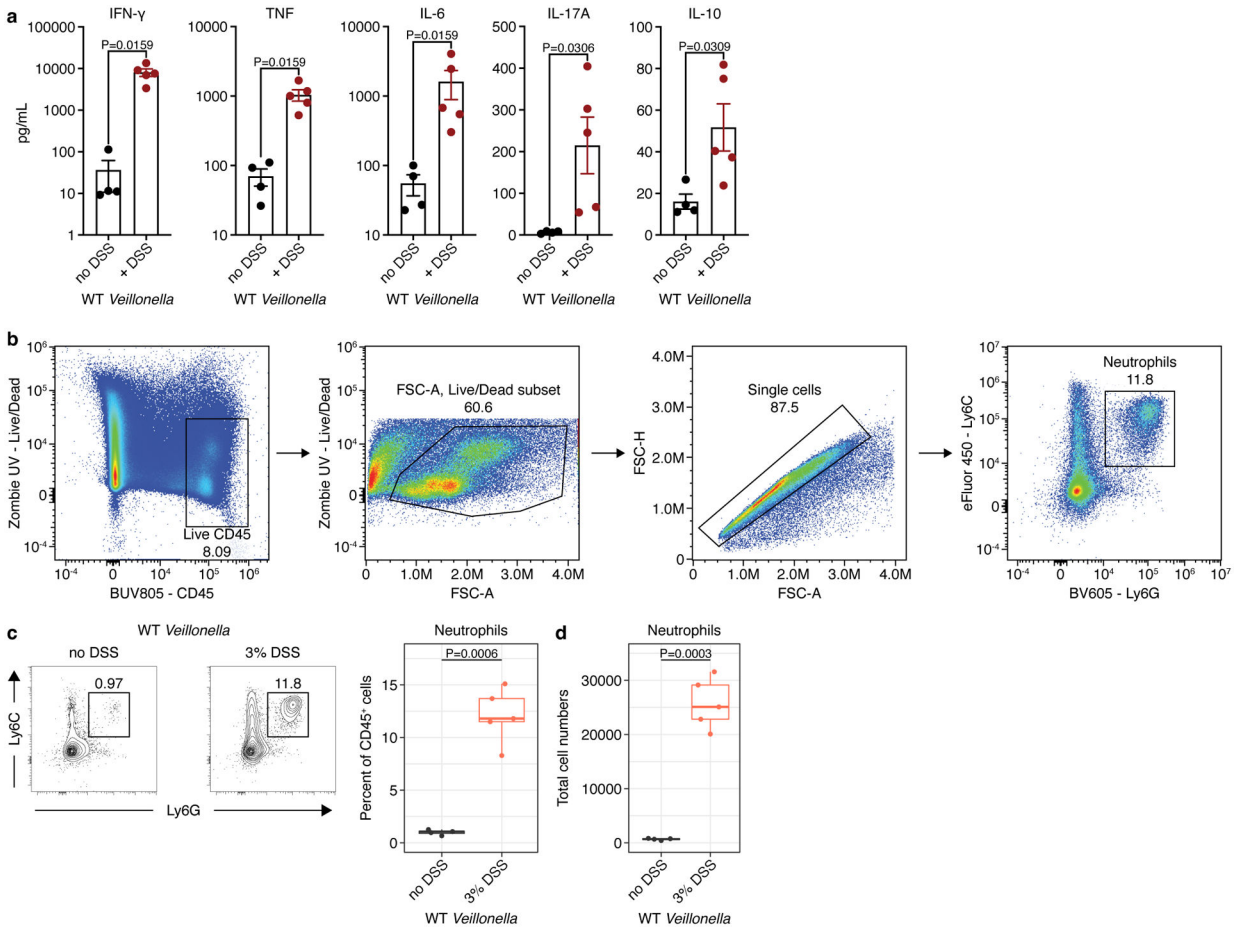

Extended Data Figure 8. Validation of the DSS-treated mouse model.

a) Measurements of IFN-γ, TNF, IL-6, IL-17A, and IL-10 in the mesenteric lymph nodes of WT-colonized ASF mice without (n=4) and with (n=5) DSS treatment. **b)** Lamina propria cells were isolated from colonic tissue and analyzed via flow cytometry. From left to right: Cells were first gated for positive expression of the pan immune cell marker CD45 while excluding dead cells staining for the viability dye Zombie UV. Next, gating was further cleaned by gating on FSC-A to exclude debris and FSC-A versus FSC-H to exclude doublets. Finally neutrophils were gated based on double positive expression of the two surface protein markers Ly6G and Ly6C. **c)** Left: representative contour plots showing the proportion of neutrophils based on positive expression of Ly6C and Ly6G on live $CD45^+$ lymphocytes isolated from mouse colonic lamina propria. Right: Frequency of neutrophils among total $CD45^+$ colonic lamina propria lymphocytes. **d)** Total number of neutrophils isolated from mouse colons based on gating in **c**. The data in **a, c,** and **d** are representative of two independent experiments. For **c** and **d**, boxplots display the first and third quartiles with a thick line representing the median; n=4 mice without DSS, and n=5 mice with DSS treatment. A Student's *t*-test was used in **a**, **c**, and **d** for statistical analyses.

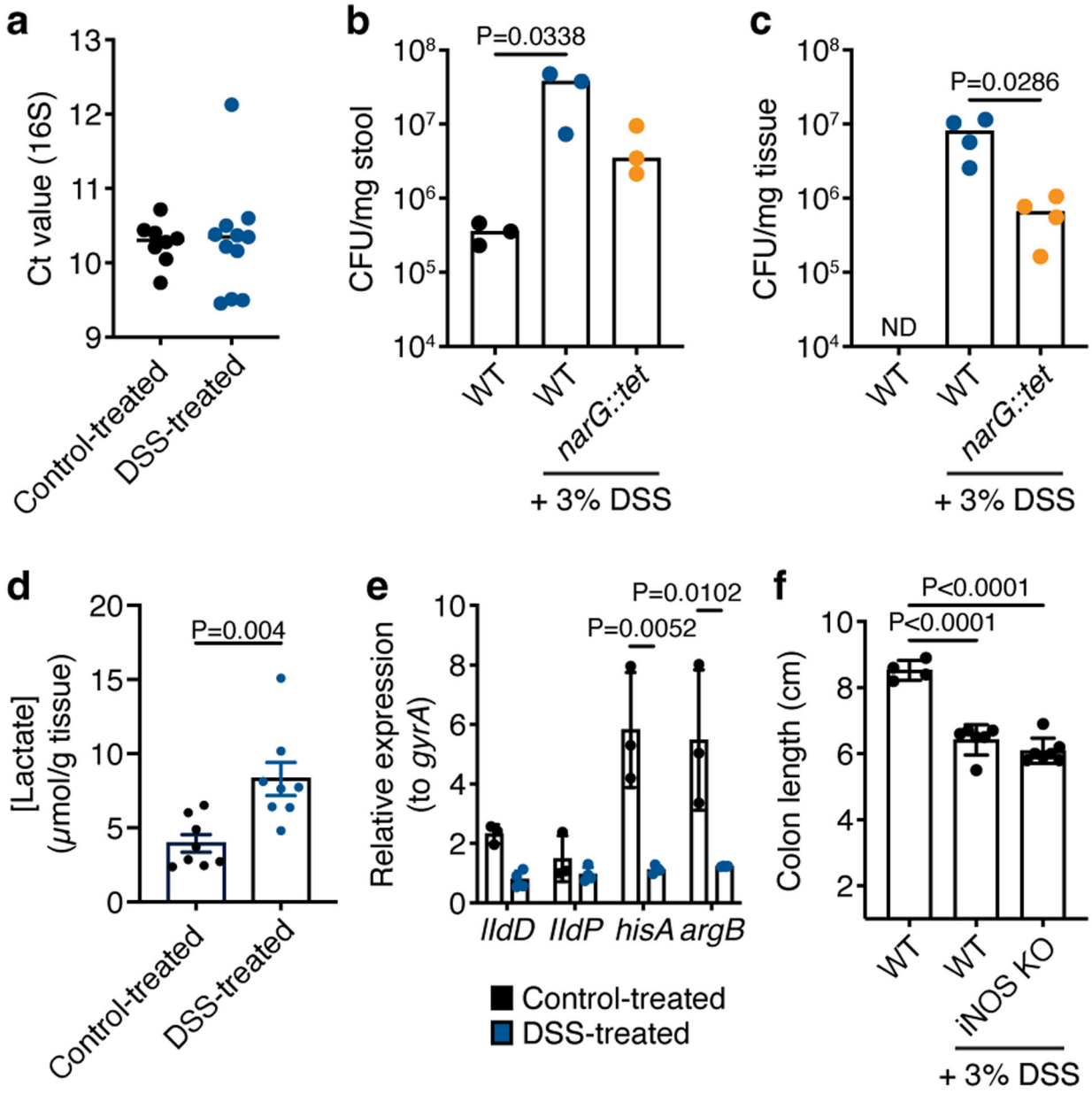

Extended Data Figure 9. Colonization of *Veillonella* in a mouse model of colitis.

a) Raw Ct values of the *Veillonella* 16S rRNA gene measured by qPCR in the stool of WT-colonized ASF mice with and without DSS treatment (n=8–11 mice). **b)** Absolute abundance of *Veillonella* in the stool of ASF mice as measured by CFU per mg of stool on selective SKLN media (n=3 mice). **c)** Absolute abundance of *Veillonella* in the colonic tissue of ASF mice as measured by CFU per mg of tissue on selective SKLN media (n=4 mice). **d)** Concentration of lactate in the gut of control- and DSS-treated ASF mice colonized with WT *Veillonella* (n=8 mice). **e)** Relative expression of the *IIdD, lldP, hisA* and *argB* genes in WT *Veillonella* colonizing the stool of mice with and without DSS treatment (n=3–4). The *gyrA* gene was used as an internal control. **f)** Colon lengths of WT and iNOS KO SPF mice (n=4–7). Data represent two independent experiments and show mean (**a, d-f**)

± SEM (**d-f**) or median (**b,c**) values. Data were analyzed by one-way ANOVA and Tukey's HSD test or Mann-Whitney *U-test*.

Supplementary Material

Refer to Web version on PubMed Central for supplementary material.

ACKNOWLEDGMENTS

We deeply thank Justin L. Merritt at Oregon Health & Science University for the SKV38 strain of *Veillonella parvula* and the pBSLJ1 plasmid, as well as José Vargas Asencio at MIT for helpful discussions, and Theresa Reimels for editorial assistance. RNA-sequencing libraries were constructed and sequenced at the Broad Institute of MIT and Harvard by the Microbial 'Omics Core and Genomics Platform, respectively. The Microbial 'Omics Core also provided preliminary analysis for all RNA-sequencing data. We thank the gnotobiotic animal facility at the Broad Institute, specifically Carlos Umana and Allan Discua for helping with experiments and Tyler Caron for providing support for running the facility. This work was supported by grants from the National Institutes of Health (P30 DK043351), Center for Microbiome Informatics and Therapeutics, and Crohn's and Colitis Foundation to R.J.X and from the Deutsche Forschungsgemeinschaft (DFG, German Research Foundation, 426120468) to M.S.

DATA AVAILABILITY

RNA-sequencing data is available on the Sequence Read Archive (SRA) under BioProject ID PRJNA838968. Source data are provided with this paper. Human microbiome data was accessed through data deposited on the SRA under BioProject ID PRJNA436359.

CODE AVAILABILITY

No custom code was generated or used in this study.

REFERENCES

1. Lamont RJ, Koo H & Hajishengallis G The oral microbiota: dynamic communities and host interactions. Nat Rev Microbiol 16, 745–759, doi:10.1038/s41579-018-0089-x (2018). [PubMed: 30301974]
2. Dewhirst FE et al. The human oral microbiome. J Bacteriol 192, 5002–5017, doi:10.1128/JB.00542-10 (2010). [PubMed: 20656903]
3. Kitamoto S et al. The Intermucosal Connection between the Mouth and Gut in Commensal Pathobiont-Driven Colitis. Cell 182, 447–462 e414, doi:10.1016/j.cell.2020.05.048 (2020). [PubMed: 32758418]
4. Atarashi K et al. Ectopic colonization of oral bacteria in the intestine drives TH1 cell induction and inflammation. Science 358, 359–365, doi:10.1126/science.aan4526 (2017). [PubMed: 29051379]
5. Gevers D et al. The treatment-naive microbiome in new-onset Crohn's disease. Cell Host Microbe 15, 382–392, doi:10.1016/j.chom.2014.02.005 (2014). [PubMed: 24629344]
6. Shaw KA et al. Dysbiosis, inflammation, and response to treatment: a longitudinal study of pediatric subjects with newly diagnosed inflammatory bowel disease. Genome Med 8, 75, doi:10.1186/s13073-016-0331-y (2016). [PubMed: 27412252]
7. Ananthakrishnan AN et al. Gut Microbiome Function Predicts Response to Anti-integrin Biologic Therapy in Inflammatory Bowel Diseases. Cell Host Microbe 21, 603–610 e603, doi:10.1016/j.chom.2017.04.010 (2017). [PubMed: 28494241]
8. Santoru ML et al. Cross sectional evaluation of the gut-microbiome metabolome axis in an Italian cohort of IBD patients. Sci Rep 7, 9523, doi:10.1038/s41598-017-10034-5 (2017). [PubMed: 28842640]
9. Geng J et al. Co-occurrence of driver and passenger bacteria in human colorectal cancer. Gut Pathog 6, 26, doi:10.1186/1757-4749-6-26 (2014). [PubMed: 24995042]

10. Kostic AD et al. Fusobacterium nucleatum potentiates intestinal tumorigenesis and modulates the tumor-immune microenvironment. Cell Host Microbe 14, 207–215, doi:10.1016/j.chom.2013.07.007 (2013). [PubMed: 23954159]
11. Flemer B et al. The oral microbiota in colorectal cancer is distinctive and predictive. Gut 67, 1454–1463, doi:10.1136/gutjnl-2017-314814 (2018). [PubMed: 28988196]
12. Tunney MM et al. Detection of anaerobic bacteria in high numbers in sputum from patients with cystic fibrosis. Am J Respir Crit Care Med 177, 995–1001, doi:10.1164/rccm.200708-1151OC (2008). [PubMed: 18263800]
13. Rogers GB et al. characterization of bacterial community diversity in cystic fibrosis lung infections by use of 16s ribosomal DNA terminal restriction fragment length polymorphism profiling. J Clin Microbiol 42, 5176–5183, doi:10.1128/JCM.42.11.5176-5183.2004 (2004). [PubMed: 15528712]
14. Rogers GB, Skelton S, Serisier DJ, van der Gast CJ & Bruce KD Determining cystic fibrosis-affected lung microbiology: comparison of spontaneous and serially induced sputum samples by use of terminal restriction fragment length polymorphism profiling. J Clin Microbiol 48, 78–86, doi:10.1128/JCM.01324-09 (2010). [PubMed: 19906901]
15. Seedorf H et al. Bacteria from diverse habitats colonize and compete in the mouse gut. Cell 159, 253–266, doi:10.1016/j.cell.2014.09.008 (2014). [PubMed: 25284151]
16. Hove H & Mortensen PB Influence of intestinal inflammation (IBD) and small and large bowel length on fecal short-chain fatty acids and lactate. Dig Dis Sci 40, 1372–1380, doi:10.1007/BF02065554 (1995). [PubMed: 7781463]
17. Franzosa EA et al. Gut microbiome structure and metabolic activity in inflammatory bowel disease. Nat Microbiol 4, 293–305, doi:10.1038/s41564-018-0306-4 (2019). [PubMed: 30531976]
18. Schicho R et al. Quantitative metabolomic profiling of serum, plasma, and urine by (1)H NMR spectroscopy discriminates between patients with inflammatory bowel disease and healthy individuals. J Proteome Res 11, 3344–3357, doi:10.1021/pr300139q (2012). [PubMed: 22574726]
19. Winter SE et al. Host-derived nitrate boosts growth of E. coli in the inflamed gut. Science 339, 708–711, doi:10.1126/science.1232467 (2013). [PubMed: 23393266]
20. Hughes ER et al. Microbial Respiration and Formate Oxidation as Metabolic Signatures of Inflammation-Associated Dysbiosis. Cell Host Microbe 21, 208–219, doi:10.1016/j.chom.2017.01.005 (2017). [PubMed: 28182951]
21. Winter SE et al. Gut inflammation provides a respiratory electron acceptor for Salmonella. Nature 467, 426–429, doi:10.1038/nature09415 (2010). [PubMed: 20864996]
22. Gillis CC et al. Dysbiosis-Associated Change in Host Metabolism Generates Lactate to Support Salmonella Growth. Cell Host Microbe 23, 54–64 e56, doi:10.1016/j.chom.2017.11.006 (2018). [PubMed: 29276172]
23. Thiennimitr P et al. Intestinal inflammation allows Salmonella to use ethanolamine to compete with the microbiota. Proc Natl Acad Sci U S A 108, 17480–17485, doi:10.1073/pnas.1107857108 (2011). [PubMed: 21969563]
24. Lopez CA, Rivera-Chavez F, Byndloss MX & Baumler AJ The Periplasmic Nitrate Reductase NapABC Supports Luminal Growth of Salmonella enterica Serovar Typhimurium during Colitis. Infect Immun 83, 3470–3478, doi:10.1128/IAI.00351-15 (2015). [PubMed: 26099579]
25. Lopez CA et al. Phage-mediated acquisition of a type III secreted effector protein boosts growth of salmonella by nitrate respiration. mBio 3, doi:10.1128/mBio.00143-12 (2012).
26. Hughes CV, Kolenbrander PE, Andersen RN & Moore LV Coaggregation properties of human oral Veillonella spp.: relationship to colonization site and oral ecology. Appl Environ Microbiol 54, 1957–1963, doi:10.1128/aem.54.8.1957-1963.1988 (1988). [PubMed: 3178207]
27. Mashima I & Nakazawa F The interaction between Streptococcus spp. and Veillonella tobetsuensis in the early stages of oral biofilm formation. J Bacteriol 197, 2104–2111, doi:10.1128/JB.02512-14 (2015). [PubMed: 25917902]
28. van der Hoeven JS, Toorop AI & Mikx RH Symbiotic relationship of Veillonella alcalescens and Streptococcus mutans in dental plaque in gnotobiotic rats. Caries Res 12, 142–147, doi:10.1159/000260324 (1978). [PubMed: 272950]

29. Mikx FH & Van der Hoeven JS Symbiosis of Streptococcus mutans and Veillonella alcalescens in mixed continuous cultures. Arch Oral Biol 20, 407–410, doi:10.1016/0003-9969(75)90224-1 (1975). [PubMed: 1096856]
30. Periasamy S & Kolenbrander PE Central role of the early colonizer Veillonella sp. in establishing multispecies biofilm communities with initial, middle, and late colonizers of enamel. J Bacteriol 192, 2965–2972, doi:10.1128/JB.01631-09 (2010). [PubMed: 20154130]
31. Delwiche EA, Pestka JJ & Tortorello ML The veillonellae: gram-negative cocci with a unique physiology. Annu Rev Microbiol 39, 175–193, doi:10.1146/annurev.mi.39.100185.001135 (1985). [PubMed: 3904599]
32. Schirmer M et al. Compositional and Temporal Changes in the Gut Microbiome of Pediatric Ulcerative Colitis Patients Are Linked to Disease Course. Cell Host Microbe 24, 600–610 e604, doi:10.1016/j.chom.2018.09.009 (2018). [PubMed: 30308161]
33. Kugathasan S et al. Prediction of complicated disease course for children newly diagnosed with Crohn's disease: a multicentre inception cohort study. Lancet 389, 1710–1718, doi:10.1016/S0140-6736(17)30317-3 (2017). [PubMed: 28259484]
34. Rogosa M The Genus Veillonella. I. General Cultural, Ecological, and Biochemical Considerations. J Bacteriol 87, 162–170, doi:10.1128/jb.87.1.162-170.1964 (1964). [PubMed: 14102850]
35. Doel JJ, Benjamin N, Hector MP, Rogers M & Allaker RP Evaluation of bacterial nitrate reduction in the human oral cavity. Eur J Oral Sci 113, 14–19, doi:10.1111/j.1600-0722.2004.00184.x (2005). [PubMed: 15693824]
36. Inderlied CB & Delwiche EA Nitrate reduction and the growth of Veillonella alcalescens. J Bacteriol 114, 1206–1212, doi:10.1128/jb.114.3.1206-1212.1973 (1973). [PubMed: 4145863]
37. Mitsui T, Saito M & Harasawa R Salivary nitrate-nitrite conversion capacity after nitrate ingestion and incidence of Veillonella spp. in elderly individuals. J Oral Sci 60, 405–410, doi:10.2334/josnusd.17-0337 (2018). [PubMed: 30101819]
38. Wicaksono DP, Washio J, Abiko Y, Domon H & Takahashi N Nitrite Production from Nitrate and Its Link with Lactate Metabolism in Oral Veillonella spp. Appl Environ Microbiol 86, doi:10.1128/AEM.01255-20 (2020).
39. Moreno-Vivian C, Cabello P, Martinez-Luque M, Blasco R & Castillo F Prokaryotic nitrate reduction: molecular properties and functional distinction among bacterial nitrate reductases. J Bacteriol 181, 6573–6584, doi:10.1128/JB.181.21.6573-6584.1999 (1999). [PubMed: 10542156]
40. Knapp S et al. Natural Competence Is Common among Clinical Isolates of Veillonella parvula and Is Useful for Genetic Manipulation of This Key Member of the Oral Microbiome. Front Cell Infect Microbiol 7, 139, doi:10.3389/fcimb.2017.00139 (2017). [PubMed: 28473967]
41. Reuss O & Morschhauser J A family of oligopeptide transporters is required for growth of Candida albicans on proteins. Mol Microbiol 60, 795–812, doi:10.1111/j.1365-2958.2006.05136.x (2006). [PubMed: 16629678]
42. Berntsson RP et al. The structural basis for peptide selection by the transport receptor OppA. EMBO J 28, 1332–1340, doi:10.1038/emboj.2009.65 (2009). [PubMed: 19300437]
43. de Vries W, Rietveld-Struijk RM & Stouthamer AH ATP formation associated with fumarate and nitrate reduction in growing cultures of Veillonella alcalescens. Antonie Van Leeuwenhoek 43, 153–167, doi:10.1007/BF00395670 (1977). [PubMed: 202192]
44. Galivan JH & Allen SH Methylmalonyl coenzyme A decarboxylase. Its role in succinate decarboxylation by Micrococcus lactilyticus. J Biol Chem 243, 1253–1261 (1968). [PubMed: 5646172]
45. de Vries W, van Wijck-Kapteyn WM & Oosterhuis SK The presence and function of cytochromes in Selenomonas ruminantium, Anaerovibrio lipolytica and Veillonella alcalescens. J Gen Microbiol 81, 69–78, doi:10.1099/00221287-81-1-69 (1974). [PubMed: 4362619]
46. McCormick NG, Ordal EJ & Whiteley HR DEGRADATION OF PYRUVATE BY MICROCOCCUS LACTILYTICUS I. : General Properties of the Formate-Exchange Reaction. J Bacteriol 83, 887–898, doi:10.1128/jb.83.4.887-898.1962 (1962). [PubMed: 16561936]
47. Griffith MJ & Nishimura JS Acetate kinase from Veillonella alcalescens. Purification and physical properties. J Biol Chem 254, 442–446 (1979). [PubMed: 216674]

48. Pelroy RA & Whiteley HR Regulatory properties of acetokinase from Veillonella alcalescens. J Bacteriol 105, 259–267, doi:10.1128/jb.105.1.259-267.1971 (1971). [PubMed: 5541011]
49. Bowman CM, Valdez RO & Nishimura JS Acetate kinase from Veillonella alcalescens. Regulation of enzyme activity by succinate and substrates. J Biol Chem 251, 3117–3121 (1976). [PubMed: 178662]
50. Kolios G, Valatas V & Ward SG Nitric oxide in inflammatory bowel disease: a universal messenger in an unsolved puzzle. Immunology 113, 427–437, doi:10.1111/j.1365-2567.2004.01984.x (2004). [PubMed: 15554920]
51. Anderson CJ et al. Microbes exploit death-induced nutrient release by gut epithelial cells. Nature 596, 262–267, doi:10.1038/s41586-021-03785-9 (2021). [PubMed: 34349263]
52. Madej M et al. Structural and functional insights into oligopeptide acquisition by the RagAB transporter from Porphyromonas gingivalis. Nat Microbiol 5, 1016–1025, doi:10.1038/s41564-020-0716-y (2020). [PubMed: 32393857]
53. Pucino V et al. Lactate Buildup at the Site of Chronic Inflammation Promotes Disease by Inducing CD4(+) T Cell Metabolic Rewiring. Cell Metab 30, 1055–1074 e1058, doi:10.1016/j.cmet.2019.10.004 (2019). [PubMed: 31708446]
54. Dalgaard P & Koutsoumanis K Comparison of maximum specific growth rates and lag times estimated from absorbance and viable count data by different mathematical models. J Microbiol Methods 43, 183–196, doi:10.1016/s0167-7012(00)00219-0 (2001). [PubMed: 11118653]
55. Pasolli E et al. Extensive Unexplored Human Microbiome Diversity Revealed by Over 150,000 Genomes from Metagenomes Spanning Age, Geography, and Lifestyle. Cell 176, 649–662 e620, doi:10.1016/j.cell.2019.01.001 (2019). [PubMed: 30661755]
56. Edgar RC Search and clustering orders of magnitude faster than BLAST. Bioinformatics 26, 2460–2461, doi:10.1093/bioinformatics/btq461 (2010). [PubMed: 20709691]
57. Segata N, Bornigen D, Morgan XC & Huttenhower C PhyloPhlAn is a new method for improved phylogenetic and taxonomic placement of microbes. Nat Commun 4, 2304, doi:10.1038/ncomms3304 (2013). [PubMed: 23942190]
58. Shishkin AA et al. Simultaneous generation of many RNA-seq libraries in a single reaction. Nat Methods 12, 323–325, doi:10.1038/nmeth.3313 (2015). [PubMed: 25730492]
59. Zhu YY, Machleder EM, Chenchik A, Li R & Siebert PD Reverse transcriptase template switching: a SMART approach for full-length cDNA library construction. Biotechniques 30, 892–897, doi:10.2144/01304pf02 (2001). [PubMed: 11314272]
60. Li H & Durbin R Fast and accurate short read alignment with Burrows-Wheeler transform. Bioinformatics 25, 1754–1760, doi:10.1093/bioinformatics/btp324 (2009). [PubMed: 19451168]
61. Robinson MD, McCarthy DJ & Smyth GK edgeR: a Bioconductor package for differential expression analysis of digital gene expression data. Bioinformatics 26, 139–140, doi:10.1093/bioinformatics/btp616 (2010). [PubMed: 19910308]
62. Abeel T, Van Parys T, Saeys Y, Galagan J & Van de Peer Y GenomeView: a next-generation genome browser. Nucleic Acids Res 40, e12, doi:10.1093/nar/gkr995 (2012). [PubMed: 22102585]
63. Mascanfroni ID et al. Metabolic control of type 1 regulatory T cell differentiation by AHR and HIF1-alpha. Nat Med 21, 638–646, doi:10.1038/nm.3868 (2015). [PubMed: 26005855]
64. Ng SK & Hamilton IR Lactate metabolism by Veillonella parvula. J Bacteriol 105, 999–1005, doi:10.1128/jb.105.3.999-1005.1971 (1971). [PubMed: 4323300]

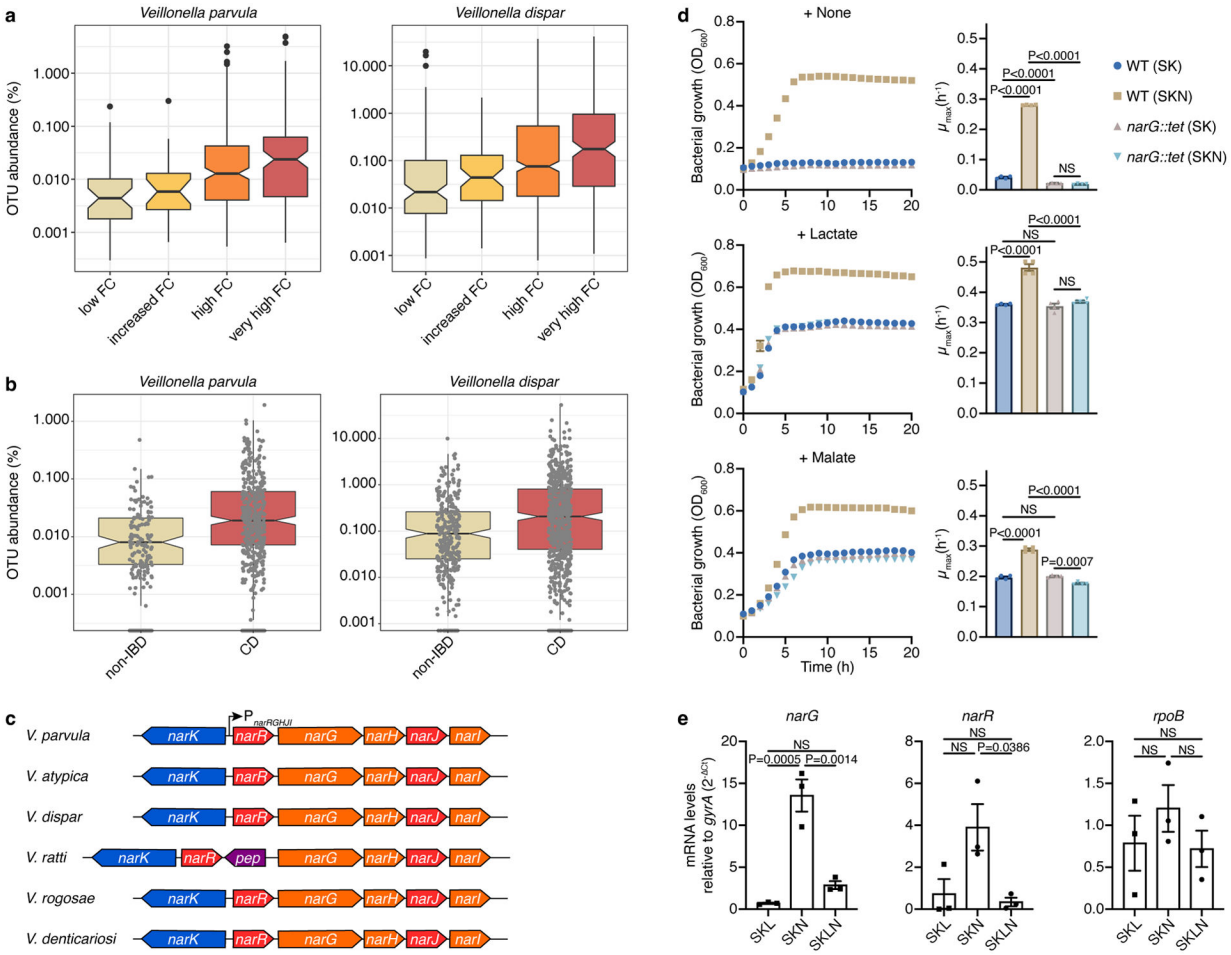

Figure 1. The abundance of nitrate-respiring *Veillonella* is increased during inflammatory bowel diseases.

a) Abundances of *V. parvula* (n=487 samples) and *V. dispar* (n=1,006 samples) from a pediatric UC cohort increase with higher levels of inflammation, as measured by fecal calprotectin (FC) concentration: low (<100 mcg/g), increased (100–200), high (200–3,000), or very high (>3,000). **b)** *V. parvula* (n=529 samples) and *V. dispar* (n=846 samples) abundances are increased in new-onset CD patients. **c)** Organization of the *narK-narR-narGHJI* cluster in *Veillonella* species. The cluster in *V. ratti* additionally includes a gene encoding a putative peptidase. **d)** Growth (measured by optical density at 600nm, OD_{600}) of wild-type (WT) and *narG::tet V. parvula* was studied for 20 h in SK medium with or without nitrate (SKN and SK, respectively) and lactate or malate as the carbon source. Maximum-specific growth rates (μ_{max}) were calculated for each growth curve (n=4 biological replicates). **e)** Comparative analysis of expression profiles of the *narG*, *narR*, and *rpoB* genes by real-time quantitative reverse transcription PCR (RT-qPCR) during growth on SK medium supplemented with lactate (SKL), nitrate (SKN), or both (SKLN). *gyrA* was the internal reference. WT cells were collected at the mid-exponential phase (n=3 biological replicates). Boxplots (**a,b**) display median, 25th and 75th percentiles, where **a** shows outliers and **b** shows all data points; data were analyzed by two-sided Wilcoxon test. Data (**d,e**)

represent mean±SEM (standard error of the mean), analyzed by one-way ANOVA and Tukey's honestly significant difference (HSD) test. NS, not significant.

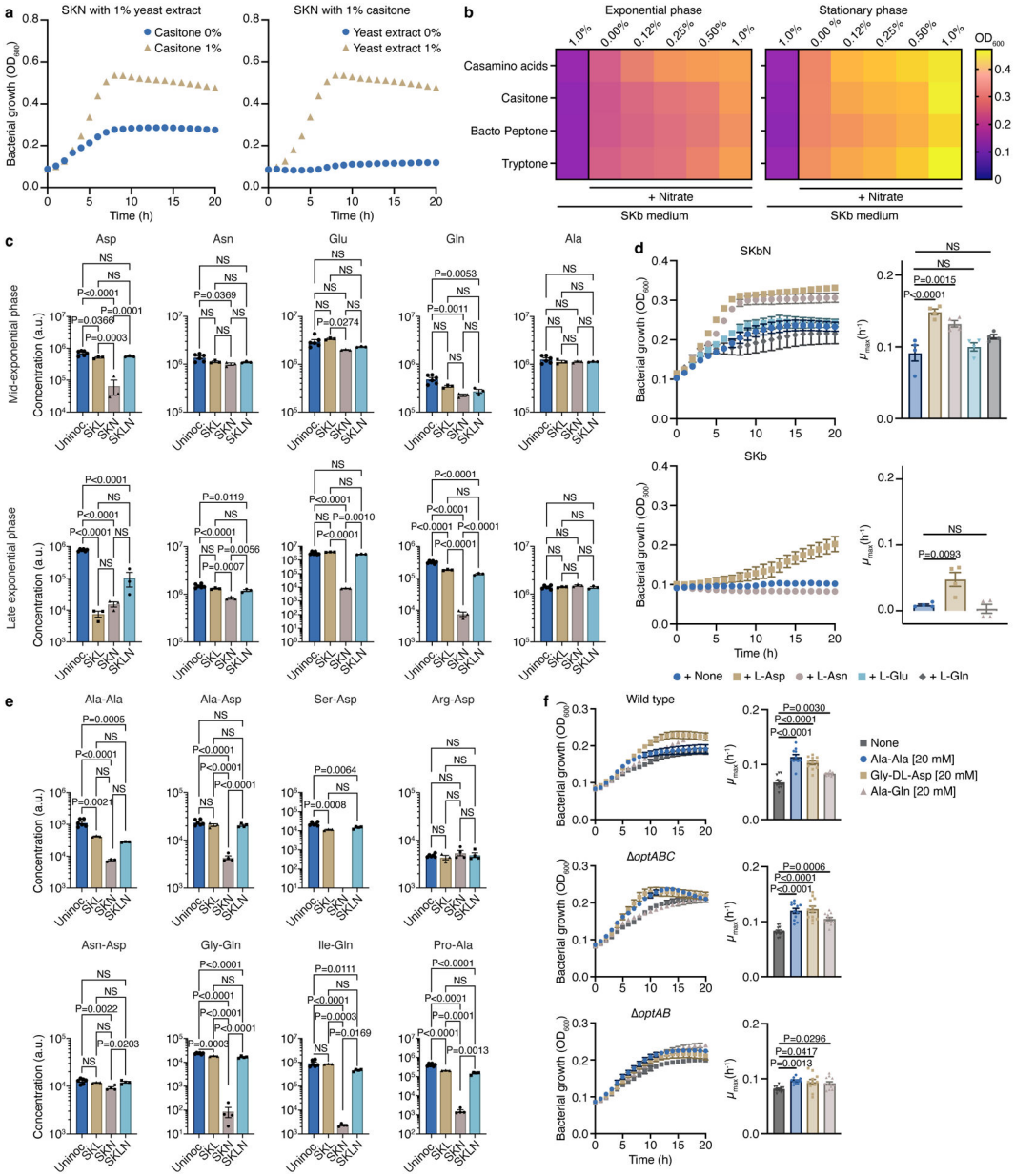

Figure 2. Nitrate respiration expands the metabolic repertoire of *Veillonella*.

WT growth in **a)** SKN lacking casitone or yeast extract (n=3) and **b)** SK base (SKb) with or without nitrate and increasing concentrations of casamino acids, casitone, bacto peptone, or tryptone (n=4). **c)** Amino acid composition in uninoculated SK (n=6) and spent SKL, SKN, and SKLN (n=3) media at mid- and late exponential phases. **d)** WT growth in SKb plus nitrate (SKbN) and SKb with or without the indicated amino acids (25mM) (n=4). **e)** Dipeptide consumption in uninoculated SK (n=6) and spent SKL, SKN, and SKLN (n=3) media at the late exponential phase. **f)** WT (n=12), *oppABC* (n=12), and *optAB* (n=11) growth in SKbN with or without the indicated dipeptides (20 mM). Growth rates (μ_{max}) were calculated for each growth curve (**d,f**). Data (**c-f**) represent mean±SEM, analyzed by

one-way ANOVA and Tukey's HSD test. NS, not significant. N numbers denote biological replicates.

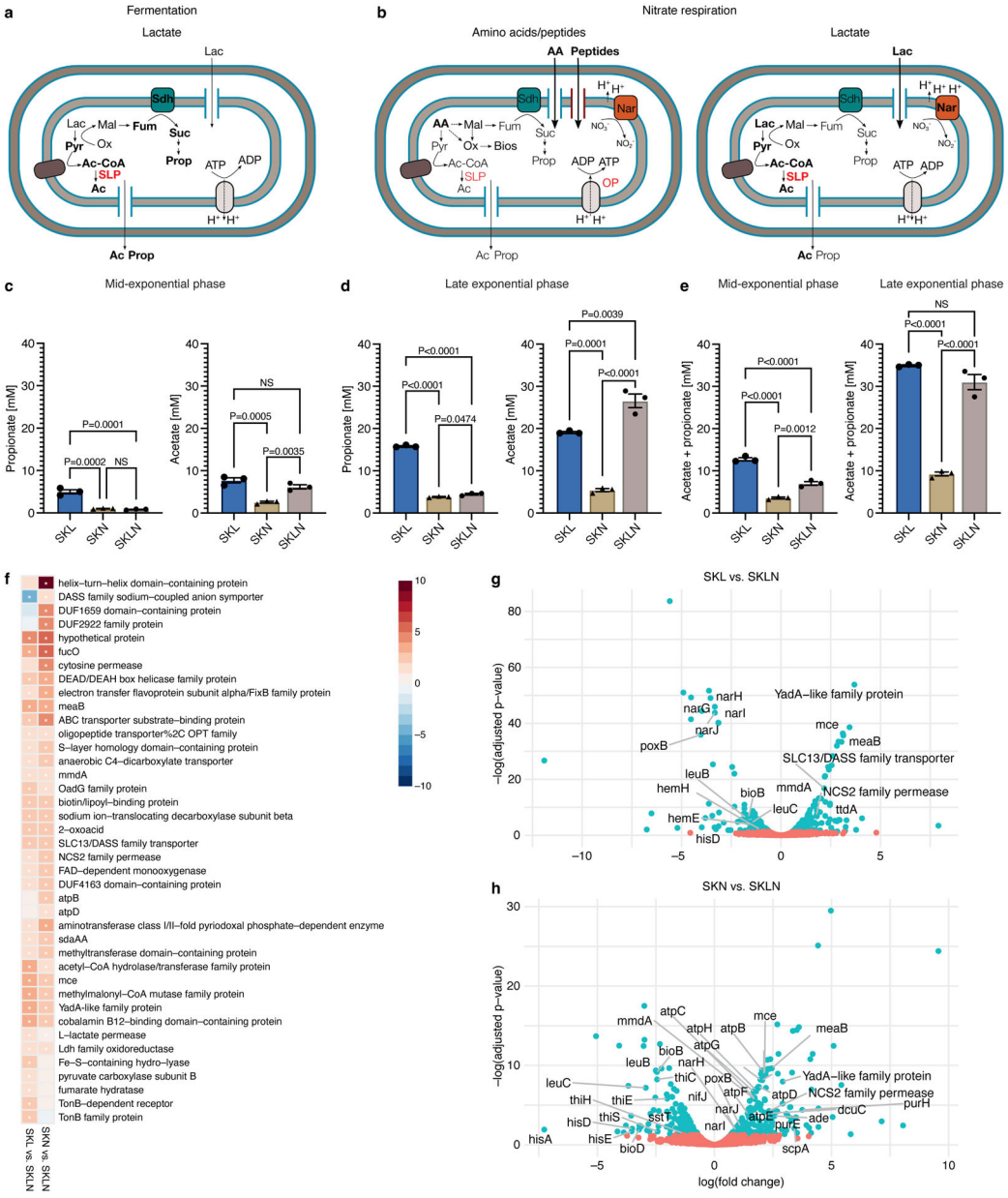

Figure 3. Metabolic changes associated with nitrate respiration.

Veillonella metabolism during **a)** lactate fermentation and **b)** nitrate respiration. Propionate and acetate concentrations in SKL, SKN, and SKLN media during **c)** mid-exponential (n=3) and **d)** late exponential (n=3) phases. Propionate and acetate concentrations in uninoculated SK medium: 0.230±0.047mM and 0.885±0.042mM, respectively (n=6). **e)** Total amount of propionate plus acetate (n=3). **f)** Transcriptomics of WT cells growing in SK with nitrate and/or lactate (n=3), ordered by statistical significance. Heatmap indicates log(fold-change). Blue, downregulated in SKL or SKN. Red, upregulated in SKL or SKN. *, significance at false discovery rate (FDR) <0.05. Differential gene expression in cells growing in **g)** SKL vs. SKLN and **h)** SKN vs. SKLN. Points represent genes colored by significance: Red, FDR>0.05. Blue, FDR<0.05. Select genes illustrate metabolic pathways of interest. Data

(**c-e**) represent mean±SEM, analyzed by one-way ANOVA and Tukey's HSD test. NS, not significant. N numbers denote biological replicates.

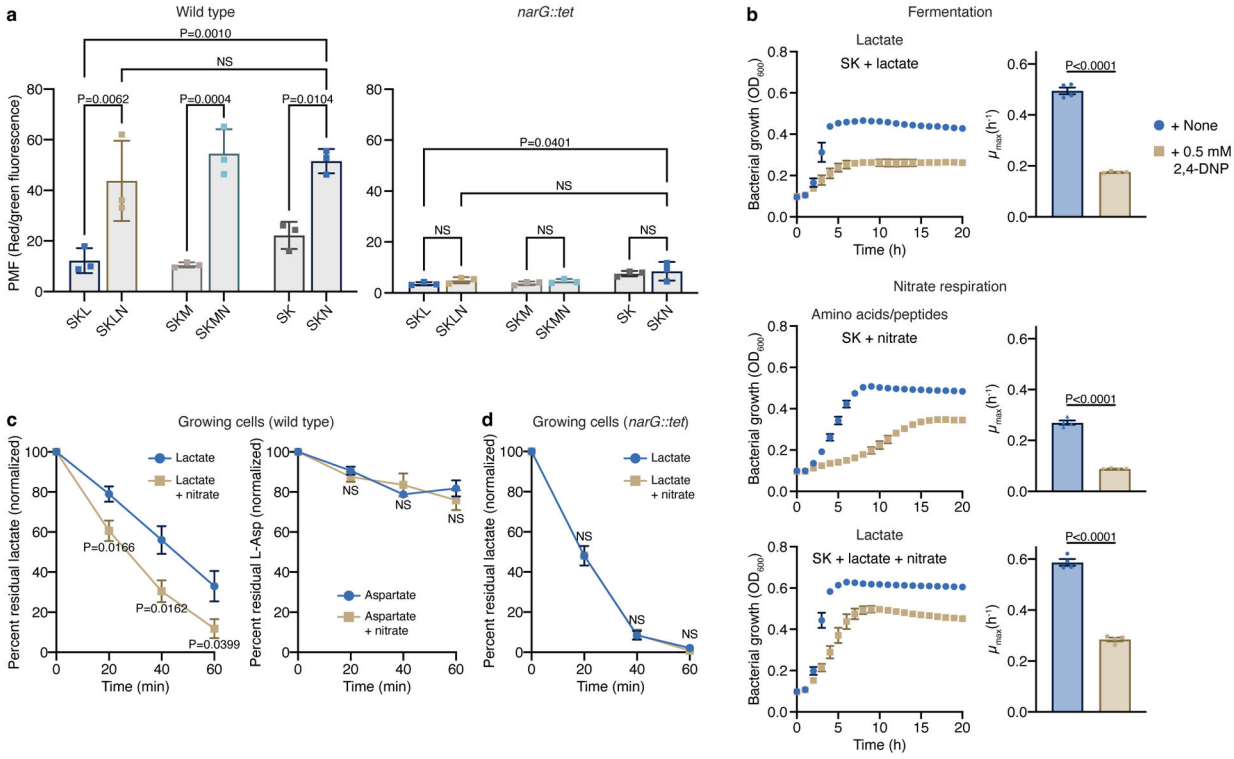

Figure 4. Nitrate respiration-mediated changes in membrane potential are harnessed for substrate transport.

a) Measurement of the proton motive force (PMF) in WT and *narG::tet* cells growing on SK media supplemented or not with lactate or malate before and 40 min after addition of 40 mM nitrate (n=3 biological replicates). **b)** Growth of *V. parvula* in the presence of 2,4-DNP in SK and SKL media supplemented or not with nitrate (n=4 biological replicates). Growth rates (μ_{max}) were calculated for each growth curve. **c)** Lactate (n=6 biological replicates) and aspartate (n=3 biological replicates) consumption by WT growing cells was determined in the spent medium 0, 20, 40, and 60 min after the addition of these carbon sources. **d)** Lactate consumption was assessed as in **c** using the *narG::tet* strain (n=4 biological replicates). Data (**a-d**) represent mean±SEM, analyzed by one-way ANOVA and Tukey's HSD test (**a**) or two-sided *t*-test (**b-d**) . NS, not significant.

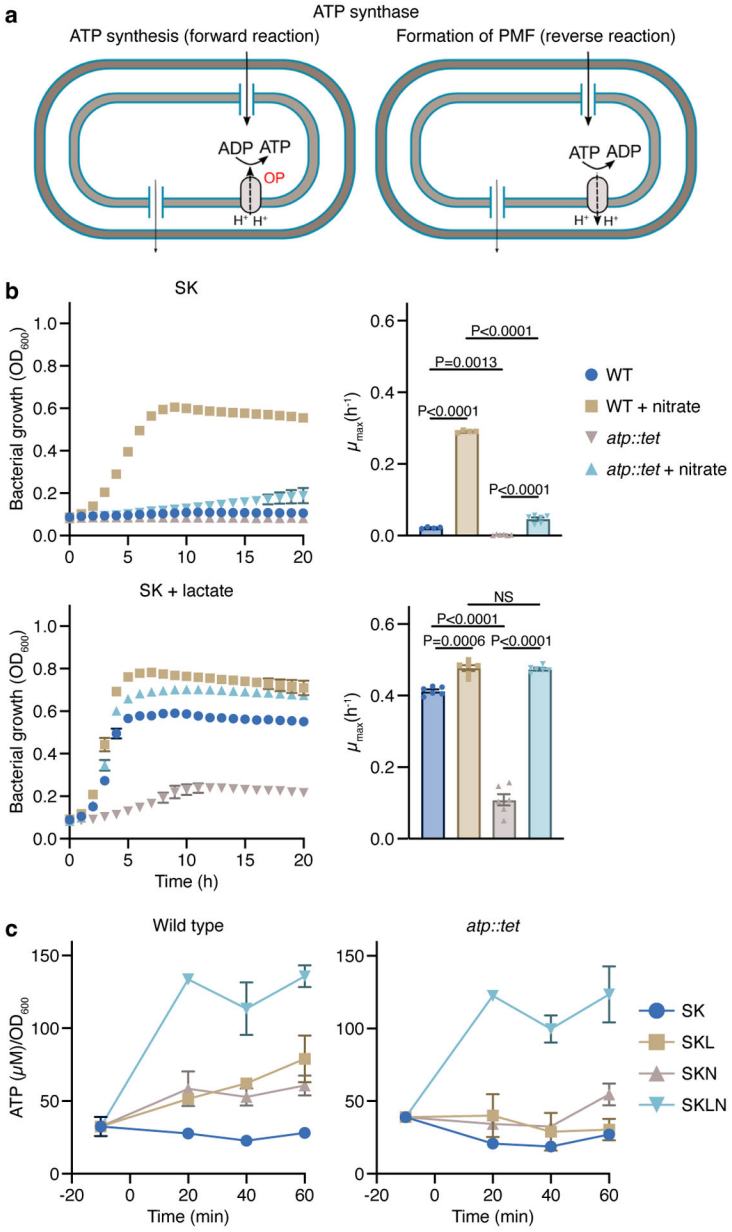

Figure 5. The conditional dispensability of ATP synthase unveils mechanistic aspects associated with fermentation and nitrate respiration.

a) The ATP synthase is a multiprotein complex that couples ATP formation to the proton motive force (forward reaction) or generates an electrochemical potential using ATP hydrolysis (reverse reaction). **b)** Growth curves of *V. parvula* lacking the ATP synthase (*atp::tet*) in the presence or absence of nitrate and/or lactate compared to WT *V. parvula* (n=4 or 6 biological replicates). Growth rates (μ_{max}) were calculated for each growth curve. **c)** Measurements of ATP in WT and *atp::tet* cells in media with and without lactate and/or nitrate (n=3 biological replicates). Data (**b,c**) represent mean±SEM, analyzed by one-way ANOVA and Tukey's HSD test. NS, not significant.

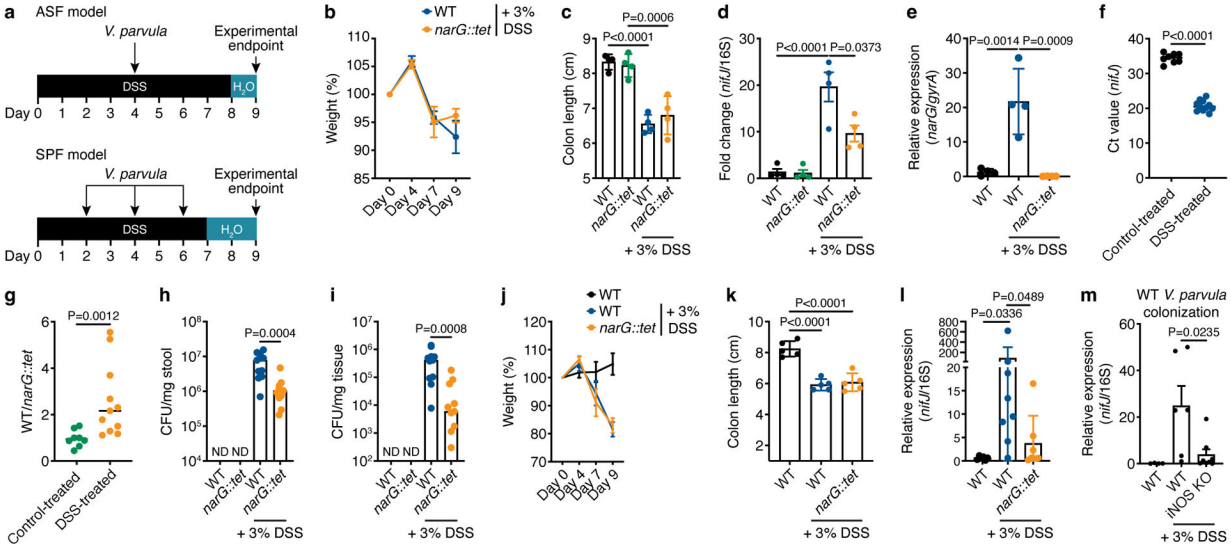

Figure 6. Nitrate reductase activity is required for efficient colonization in a mouse model of inflammation.

a) Experimental design of mouse models of colitis. Assessments of **b)** weight change over DSS treatment course and **c)** colon length at experimental endpoint (n=5). **d)** Relative abundance of *Veillonella* in stool of ASF mice, calculated using the $\Delta\Delta C(t)$ method comparing *V. parvula nifJ* and 16S rRNA genes (n=4). **e)** Relative expression of the *narG* gene in WT *Veillonella* colonizing stool of control- and DSS-treated ASF mice, with *narG::tet*-colonized mice serving as a negative control (n=4). *gyrA* was used as an internal control. **f)** Ct values of the *Veillonella nifJ* gene measured by qPCR in stool of WT-colonized ASF mice with and without DSS treatment (n=8–11). **g)** qPCR analysis of the relative colonization of WT and *narG::tet* strains in stool of ASF mice inoculated with a 1:1 mixture of each strain with and without DSS treatment (n=8–11). The y-axis represents the fold-change difference in abundance of each strain. Colony-forming units (CFUs) measured from **h)** stool and **i)** colonic tissue of ASF mice inoculated 1:1 with WT and *narG::tet* strains (n=8–11). ND, not detected. Weight change **j)** and colon length **k)** in SPF mice (n=5). **l)** Colonization of WT and *narG::tet* strains in stool of SPF mice measured by qPCR, comparing Ct values of *nifJ* and 16S rDNA (n=6–8). **m)** Colonization of WT *Veillonella* in stool of WT and iNOS KO DSS-treated SPF mice compared to control-treated WT mice measured by qPCR (n=4–8). Data represent two independent experiments and show mean (**b-g, j-m**) ± SEM (**b-e, j-m**) or median (**h,i**) values. Data was analyzed by one-way ANOVA and Tukey's HSD test or Mann-Whitney *U-test*. NS, not significant. N numbers denote mice.